

Unsupervised Linear and Nonlinear Channel Equalization and Decoding using Variational Autoencoders

Avi Caciularu and David Burshtein, *Senior Member, IEEE*

Abstract

A new approach for blind channel equalization and decoding, using variational autoencoders (VAEs), is introduced. We first consider the reconstruction of uncoded data symbols transmitted over a noisy linear intersymbol interference (ISI) channel, with an unknown impulse response, without using pilot symbols. We derive an approximated maximum likelihood estimate to the channel parameters and reconstruct the transmitted data. We demonstrate significant and consistent improvements in the error rate of the reconstructed symbols, compared to existing blind equalization methods such as constant modulus, thus enabling faster channel acquisition. The VAE equalizer uses a fully convolutional neural network with a small number of free parameters. These results are extended to blind equalization over a noisy nonlinear ISI channel with unknown parameters. We then consider coded communication using low-density parity-check (LDPC) codes transmitted over a noisy linear or nonlinear ISI channel. The goal is to reconstruct the transmitted message from the channel observations corresponding to a transmitted codeword, without using pilot symbols. We demonstrate substantial improvements compared to expectation maximization (EM) using turbo equalization. Furthermore, in our simulations we demonstrate a relatively small gap between the performance of the new unsupervised equalization method and that of the fully channel informed (non-blind) turbo equalizer.

Index Terms

Blind equalizers, maximum likelihood estimation, deep learning, convolutional neural networks, belief propagation.

I. INTRODUCTION

Deep learning methods have recently been considered in various communication problems. For example, in [1]–[4] deep learning methods were considered to the problem of channel decoding, in [5] an autoencoder for short blocklength end-to-end communications was proposed, and in [6] deep learning

This research was supported by the Israel Science Foundation (grant no. 1868/18), and by the Yitzhak and Chaya Weinstein Research Institute for Signal Processing.

A. Caciularu is with the school of Electrical Engineering, Tel-Aviv University, Tel-Aviv 6997801, Israel (email: avi.c33@gmail.com).

D. Burshtein is with the school of Electrical Engineering, Tel-Aviv University, Tel-Aviv 6997801, Israel (email: burstyn@eng.tau.ac.il).

was used for MIMO detection. Various authors have considered deep learning-based channel equalization, separately or jointly with the decoding task. In [7] deep learning-based detection algorithms were used when the channel model is unknown. In [8] the authors show improved decoding of low-density parity-check (LDPC) codes, by augmenting the belief propagation (BP) algorithm with a convolutional neural network (CNN). In [9], [10], generative adversarial networks (GANs) were proposed to model channel effects in end-to-end communication systems.

In this work, we consider transmission over a noisy intersymbol interference (ISI) channel with an unknown impulse response. The ISI channel is useful to model various communication scenarios, such as multipath in wireless channels [11]. Unlike the works that were mentioned above, we do not assume the availability of a pilot signal to learn the unknown channel. The motivation is that pilot symbols reduce the communication throughput, especially when the communication environment is changing rapidly. Instead, unsupervised (in the sense that pilot symbols are not required) blind channel equalization is proposed. For uncoded transmitted data, the standard approach for blind channel equalization is the constant modulus algorithm (CMA) [12]–[14]. Blind neural network-based algorithms using the constant modulus (CM) criterion were proposed in [15]. The maximum likelihood (ML) criterion has also been considered for blind channel equalization [16]–[20] (and references therein). Combined blind equalization and decoding using EM for the case where the transmitted data is coded was considered in [21], [22]. The proposed solutions use the EM algorithm [23] or an approximated EM, that requires an iterative application of the Bahl, Cocke, Jelinek, and Raviv (BCJR) algorithm [24] or the Viterbi algorithm. Hence, the complexities of these algorithms are exponential in the channel memory size, which may be prohibitive.

In our work we also consider nonlinear channels, where the nonlinear distortion may be due to the presence of amplifiers, converters and mixers in transmitters and receivers. Channel equalization is applied to overcome these effects and reconstruct the signal before using the channel decoder. Some authors [25]–[29] have considered the nonlinear channel equalization problem under a supervised learning setup, which requires pilot signals for training the equalizer.

In the first part of this work, which was initially presented in [30], we present a new approach for unsupervised blind channel equalization of uncoded data, transmitted over a noisy ISI channel with an unknown impulse response, without the availability of pilot symbols. The method uses variational autoencoders (VAEs) [31], [32] as a means to obtain an approximated maximum likelihood estimate to the channel parameters. VAEs are widely used in the literature of deep learning for unsupervised and semi-supervised learning, and as a generative model to a given observations data. We demonstrate significant and consistent improvements in the error rate of the reconstructed symbols, compared to existing blind equalization methods such as constant modulus, thus enabling faster channel acquisition. In fact, for the channels that were examined, the performance of the new blind VAE equalizer (VAEE) was close

to the performance of a non-blind adaptive linear minimum mean square error (MMSE) equalizer [33]. Furthermore, unlike the ML-based blind equalization methods in the literature [16]–[20], the computational complexity of our approach is not exponential in the channel memory size. In fact, the VAEE uses a fully convolutional neural network with a very small number of free parameters. Although the computational complexity of the new VAEE is higher compared to CMA, it is still reasonable, and the convergence rate is fast. These results are extended to unsupervised blind equalization over a noisy nonlinear ISI channel with unknown parameters. We then consider coded communication using LDPC codes transmitted over a noisy linear or nonlinear ISI channel. The goal is to reconstruct the transmitted message from the channel observations corresponding to a single transmitted codeword, without using pilot symbols. We demonstrate substantial improvements compared to EM using turbo equalization [34], [35]. Furthermore, in our simulations we demonstrate a relatively small gap between the performance of the new unsupervised equalization method and that of the fully channel informed (non-blind) turbo equalizer.

The rest of this paper is organized as follows. In Section II we present the problem setup considered in this paper. In Section III we present our proposed solution for uncoded data transmitted over a noisy linear ISI channel. In Section IV we consider the same setup for noisy nonlinear channels. In Section V we consider LDPC coded data transmitted over noisy (linear or nonlinear) ISI channels, and present joint blind equalization and decoding using our method. In Section VI we present simulation results. Finally, Section VII concludes this paper.

II. PROBLEM SETUP

The communication channel is modeled as a convolution of the input, $\{x_k\}$, with some causal, finite impulse response (FIR), time invariant filter, $\mathbf{h} = (h_0, h_1, \dots, h_{M-1})$, of size M , followed by the possibly nonlinear mapping $g(\cdot)$ and the addition of white Gaussian noise

$$y_n = g\left(\sum_k x_k h_{n-k}\right) + w_n \quad (1)$$

This is the equivalent model of $\{y_k\}$ in the end-to-end communication system shown in Fig. 1, where the sampling is performed at the symbol rate.

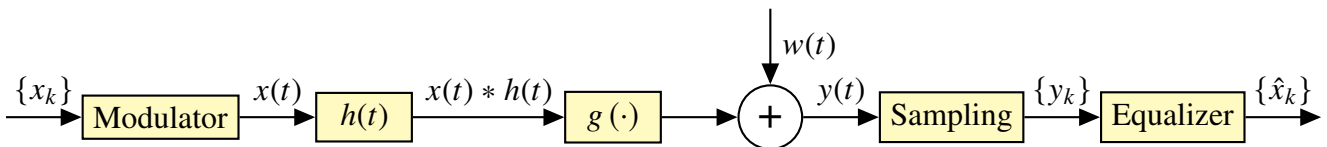


Fig. 1: End-to-end communication system model.

The equalizer in Fig. 1 reconstructs an estimate of the transmitted symbol sequence, $\{\hat{x}_k\}$. Now, suppose that we observe a finite window of measurements data $\mathbf{y} \triangleq (y_0, y_1, \dots, y_{N-1})$. For clarity of presentation,

we assume that the input signal is causal ($x_k = 0$ for $k < 0$). We refer to this assumption later. Equation (1) can be written compactly for the measurements collected in \mathbf{y} as

$$\mathbf{y} = g(\mathbf{x} * \mathbf{h}) + \mathbf{w} \quad (2)$$

where $\mathbf{x} = (x_0, x_1, \dots, x_{N-1})$ is the transmitted message, and $\mathbf{w} = (w_0, w_1, \dots, w_{N-1})$ is an i.i.d. sequence of additive white Gaussian noise. In (2), the scalar function $g(\cdot)$ is applied component-wise on $\mathbf{x} * \mathbf{h}$. Note that by setting $g(x) = x$ the model degenerates to a noisy linear ISI channel. In this paper we consider both BPSK and QPSK modulation, although the derivation can be extended to other constellations.

Our goal in this paper is to design the equalizer that reconstructs the transmitted sequence \mathbf{x} . The design utilizes only the channel observations \mathbf{y} , i.e., without knowing the channel parameters, including the impulse response \mathbf{h} , the nonlinear function $g(\cdot)$ and the noise variance. This is an unsupervised blind channel equalization problem where pilot signals are not available.

We will discuss both the case of uncoded data, $\{x_k\}$ (or when coding information is not used), and the case of coded data.

A. BPSK modulation

For BPSK modulation, $x_k = \pm 1$. We assume a uniformly distributed transmitted sequence, so that for all $\mathbf{x} \in \{-1, 1\}^N$ the probability of \mathbf{x} is given by

$$p(\mathbf{x}) = 2^{-N} \quad (3)$$

The noise, \mathbf{w} , is a sequence of independent identically distributed (i.i.d) Gaussian random variables with variance σ_w^2 . Given \mathbf{x} , \mathbf{y} is a vector of statistically independent, normally distributed components. The conditional density function of \mathbf{y} is $\mathcal{N}(g(\mathbf{x} * \mathbf{h}), \sigma_w^2 I_N)$. Thus, for $\boldsymbol{\theta} \triangleq \{\mathbf{h}, g(\cdot), \sigma_w^2\}$, the conditional density of \mathbf{y} given \mathbf{x} can be expressed as

$$\begin{aligned} p_{\boldsymbol{\theta}}(\mathbf{y} | \mathbf{x}) &= p_{\boldsymbol{\theta}}(\mathbf{y} | \mathbf{x}) \\ &= \frac{1}{(2\pi\sigma_w^2)^{N/2}} \cdot e^{-\|\mathbf{y} - g(\mathbf{x} * \mathbf{h})\|^2 / [2\sigma_w^2]} \end{aligned}$$

B. QPSK modulation

For QPSK modulation, $x_k = \pm 1 \pm j$, and the above vectors can be written as combinations of real (I) and imaginary (Q) components, so that, $\mathbf{x} = \mathbf{x}^I + j \cdot \mathbf{x}^Q$, $\mathbf{h} = \mathbf{h}^I + j \cdot \mathbf{h}^Q$ and $\mathbf{y} = \mathbf{y}^I + j \cdot \mathbf{y}^Q$. We assume a uniformly distributed transmitted sequence, so that for all valid \mathbf{x} the probability of \mathbf{x} is given by

$$p(\mathbf{x}) = p(\mathbf{x}^I)p(\mathbf{x}^Q) = 2^{-2N} \quad (4)$$

Each element of the i.i.d noise sequence, \mathbf{w} , is complex Gaussian with statistically independent real and imaginary components, each with variance $\sigma_w^2/2$. Given \mathbf{x} , \mathbf{y}^I and \mathbf{y}^Q are statistically independent, normally distributed. The conditional density function of \mathbf{y}^I is $\mathcal{N}(\Re(g(\mathbf{x} * \mathbf{h})), (\sigma_w^2/2)I_N)$. The conditional density function of \mathbf{y}^Q is $\mathcal{N}(\Im(g(\mathbf{x} * \mathbf{h})), (\sigma_w^2/2)I_N)$. Thus, for $\boldsymbol{\theta} \triangleq \{\mathbf{h}, g(\cdot), \sigma_w^2\}$, the conditional density of \mathbf{y} given \mathbf{x} can be expressed as

$$\begin{aligned} p_{\boldsymbol{\theta}}(\mathbf{y} | \mathbf{x}) &= p_{\boldsymbol{\theta}}(\mathbf{y}^I | \mathbf{x}^I) p_{\boldsymbol{\theta}}(\mathbf{y}^Q | \mathbf{x}^Q) \\ &= \frac{1}{(\pi\sigma_w^2)^N} \cdot e^{-\|\mathbf{y} - g(\mathbf{x} * \mathbf{h})\|^2 / \sigma_w^2} \end{aligned} \quad (5)$$

III. PROPOSED METHOD FOR A NOISY LINEAR ISI CHANNEL

In this section we consider the uncoded case, where coding information in $\{x_k\}$ is not used. We also assume that $g(x) = x$ (see Fig. 3) so that the channel is linear. In the next section we consider the case of a nonlinear channel. We start with the case of QPSK modulation, and then note how the results simplify for BPSK modulation.

A. QPSK modulation

We propose using ML estimation of the channel impulse response, \mathbf{h} , and noise variance, σ_w^2 . That is, we search for the vector $\boldsymbol{\theta} = (\mathbf{h}, \sigma_w^2)$ that maximizes $\log p_{\boldsymbol{\theta}}(\mathbf{y})^1$. The ML estimate has strong asymptotic optimality properties, and in particular asymptotic efficiency [17]. For the CMA criterion, on the other hand, one can only claim asymptotic consistency [36]. However, applying the exact ML criterion to our problem is very difficult since $p_{\boldsymbol{\theta}}(\mathbf{y})$ should first be expressed as

$$p_{\boldsymbol{\theta}}(\mathbf{y}) = \sum_{\mathbf{x}} p(\mathbf{x}) p_{\boldsymbol{\theta}}(\mathbf{y} | \mathbf{x}) d\mathbf{x}$$

where we sum over all 2^{2N} possible input sequences \mathbf{x} and where $p(\mathbf{x})$ is given by (4). Nevertheless, for this kind of problems, it has been shown in various applications that it is possible to dramatically simplify the estimation problem by using the VAE approach for ML estimation [31], [32]. By the VAE approach, instead of directly maximizing $p_{\boldsymbol{\theta}}(\mathbf{y})$ over $\boldsymbol{\theta}$, one maximizes a variational lower bound, also called evidence lower bound (ELBO), as follows. It can be shown [31] that

$$\begin{aligned} \log p_{\boldsymbol{\theta}}(\mathbf{y}) &\geq \mathbb{E}_{q_{\Phi}(\mathbf{x} | \mathbf{y})} [-\log q_{\Phi}(\mathbf{x} | \mathbf{y}) + \log p_{\boldsymbol{\theta}}(\mathbf{x}, \mathbf{y})] \\ &= \underbrace{-D_{KL}[q_{\Phi}(\mathbf{x} | \mathbf{y}) || p(\mathbf{x})]}_A + \underbrace{\mathbb{E}_{q_{\Phi}(\mathbf{x} | \mathbf{y})} [\log p_{\boldsymbol{\theta}}(\mathbf{y} | \mathbf{x})]}_B \triangleq -\mathcal{L}(\boldsymbol{\theta}, \Phi, \mathbf{y}) \end{aligned} \quad (6)$$

where $D_{KL}[\cdot || \cdot]$ denotes the Kullback Leibler distance between two density functions, and $q_{\Phi}(\mathbf{x} | \mathbf{y})$ is an arbitrary parametrized (by Φ) conditional density function. Now, instead of directly maximizing $p_{\boldsymbol{\theta}}(\mathbf{y})$,

¹The default base of the logarithms in this paper is e .

one maximizes the lower bound $-\mathcal{L}(\theta, \Phi, \mathbf{y})$ over θ and Φ jointly. Following [31, Fig. 1], Fig. 2 shows a directed graphical model that explains the VAE approach.

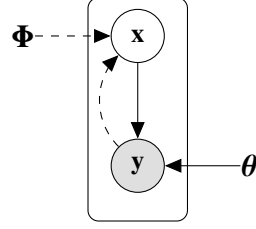


Fig. 2: A directed graphical model describing the VAE approach (following [31, Fig. 1]). The generative model $p(\mathbf{x})p_\theta(\mathbf{y}|\mathbf{x})$ is denoted by solid lines. The variational approximation $q_\Phi(\mathbf{x}|\mathbf{y})$ to the intractable posterior $p_\theta(\mathbf{x}|\mathbf{y})$ is denoted by dashed lines.

In fact, it can be shown [31] that by searching over θ and *all* possible conditional densities $q(\mathbf{x}|\mathbf{y})$, one obtains the ML estimate of θ . Typically, when using the VAE approach, both $p_\theta(\mathbf{y}|\mathbf{x})$ and $q_\Phi(\mathbf{x}|\mathbf{y})$ are implemented using neural networks. In our problem, $p(\mathbf{x})$ is given in (4), and the *encoder*, $p_\theta(\mathbf{y}|\mathbf{x})$, is given in (5) (with $g(x) = x$). We use the following model for the *decoder*, $q_\Phi(\mathbf{x}|\mathbf{y})$,

$$q_\Phi(\mathbf{x}|\mathbf{y}) = \prod_{j=0}^{N-1} q_{\Phi,j}(x_j|\mathbf{y}) = \prod_{j=0}^{N-1} q_{\Phi,j}^I(x_j^I|\mathbf{y})q_{\Phi,j}^O(x_j^O|\mathbf{y})$$

Recalling that $x_j^I \in \{-1, 1\}$ and $x_j^O \in \{-1, 1\}$, this is a multivariate Bernoulli distribution with statistical independence between components. Denoting

$$\begin{aligned} q_{\Phi,j}^I(\mathbf{y}) &\triangleq q_{\Phi,j}^I(X_j^I = 1|\mathbf{y}) \\ q_{\Phi,j}^O(\mathbf{y}) &\triangleq q_{\Phi,j}^O(X_j^O = 1|\mathbf{y}) \end{aligned}$$

we have

$$q_\Phi(\mathbf{x}|\mathbf{y}) = \prod_{j=0}^{N-1} \left(q_{\Phi,j}^I(\mathbf{y}) \right)^{(1+x_j^I)/2} \left(1 - q_{\Phi,j}^I(\mathbf{y}) \right)^{(1-x_j^I)/2} \left(q_{\Phi,j}^O(\mathbf{y}) \right)^{(1+x_j^O)/2} \left(1 - q_{\Phi,j}^O(\mathbf{y}) \right)^{(1-x_j^O)/2}$$

In our implementation of the decoder, which acts as the equalizer, we used a fully convolutional network (FCN) to implement $q_{\Phi,j}^I(\mathbf{y})$ and $q_{\Phi,j}^O(\mathbf{y})$. The network has complex convolutional layers, each with two output channels, corresponding to the real and imaginary parts of the convolution as in [37], [38]. The input and output layers are also separated to two channels corresponding to the real and imaginary components of the input, \mathbf{y} , and the output probabilities, q . The convolutional layers are both one dimensional (1D) as in [38], and with a residual connection as in [39]. The nonlinear activation function of the first layer is a SoftSign function defined by $f(x) = \frac{x}{|x|+1}$, which, in our experiments, proved to converge faster than other functions such as LeakyReLU and Tanh. The nonlinear activation function of the second layer is a sigmoid function, that ensures that the outputs are in $[0, 1]$, and so they represent valid probability values.

Note that each convolutional layer uses only one filter. Using more than one filter did not improve results. Our decoder neural network, implementing $\{q_{\Phi,j}^I(\mathbf{y}), q_{\Phi,j}^O(\mathbf{y})\}$, is depicted in Fig. 3.

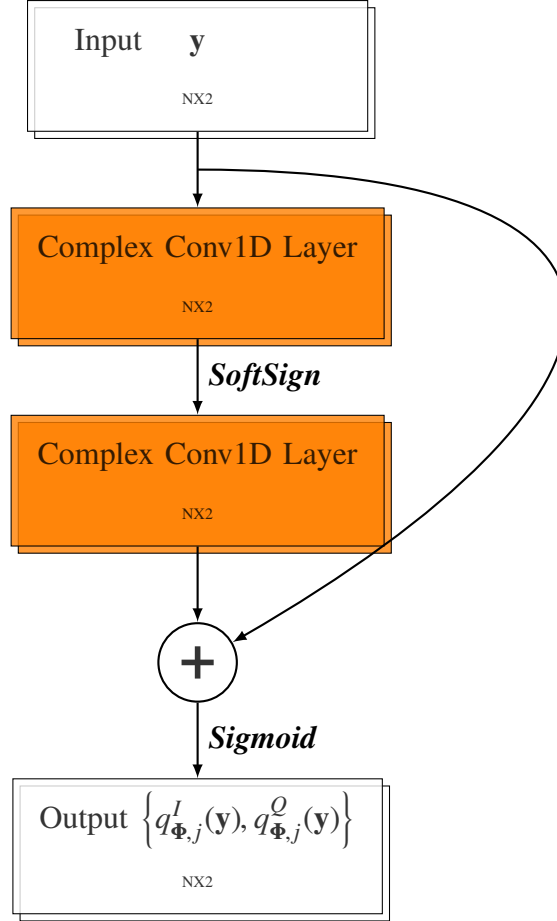


Fig. 3: Our equalizer's architecture (decoder network) using complex fully convolutional residual network. Each convolution output is listed as Width \times #Channels.

We now derive an explicit expression for the loss $\mathcal{L}(\boldsymbol{\theta}, \boldsymbol{\Phi}, \mathbf{y}) = -A - B$ (see Eq. (6)) that needs to be minimized with respect to both $\boldsymbol{\theta}$ and $\boldsymbol{\Phi}$ (alternatively, $-\mathcal{L}(\boldsymbol{\theta}, \boldsymbol{\Phi}, \mathbf{y})$ needs to be maximized).

For the term A we have

$$\begin{aligned}
 A &= \sum_{\mathbf{x}} q_{\Phi}(\mathbf{x}|\mathbf{y}) \cdot (\log p(\mathbf{x}) - \log q_{\Phi}(\mathbf{x}|\mathbf{y})) \\
 &= \sum_{\mathbf{x}} q_{\Phi}(\mathbf{x}|\mathbf{y}) \cdot (-2N \log 2 - \log q_{\Phi}(\mathbf{x}|\mathbf{y})) \\
 &= -2N \log 2 + \mathcal{H}[q_{\Phi}(\mathbf{x}|\mathbf{y})]
 \end{aligned} \tag{7}$$

where $\mathcal{H}[q_{\Phi}(\mathbf{x}|\mathbf{y})]$, the entropy of $q_{\Phi}(\mathbf{x}|\mathbf{y})$, is given by

$$\mathcal{H}[q_{\Phi}(\mathbf{x}|\mathbf{y})] = \mathcal{H}\left[\prod_{j=0}^{N-1} q_{\Phi,j}(x_j|\mathbf{y})\right] = \sum_{j=0}^{N-1} \mathcal{H}[q_{\Phi,j}(x_j|\mathbf{y})]$$

$$\begin{aligned}
&= - \sum_{j=0}^{N-1} \left[q_{\Phi,j}^I(\mathbf{y}) \log q_{\Phi,j}^I(\mathbf{y}) + \left(1 - q_{\Phi,j}^I(\mathbf{y})\right) \log \left(1 - q_{\Phi,j}^I(\mathbf{y})\right) \right. \\
&\quad \left. + q_{\Phi,j}^O(\mathbf{y}) \log q_{\Phi,j}^O(\mathbf{y}) + \left(1 - q_{\Phi,j}^O(\mathbf{y})\right) \log \left(1 - q_{\Phi,j}^O(\mathbf{y})\right) \right] \tag{8}
\end{aligned}$$

For the term B we have

$$\begin{aligned}
B &= \mathbb{E}_{q_{\Phi}(\mathbf{x}|\mathbf{y})} \left[-N \log \left(\pi \sigma_w^2 \right) - \frac{1}{\sigma_w^2} \|\mathbf{y} - \mathbf{x} * \mathbf{h}\|^2 \right] \\
&= -N \log(\pi) - N \log \left(\sigma_w^2 \right) \\
&\quad - \frac{1}{\sigma_w^2} \cdot \underbrace{\mathbb{E}_{q_{\Phi}(\mathbf{x}|\mathbf{y})} \left[\|\mathbf{y} - \mathbf{x} * \mathbf{h}\|^2 \right]}_C \tag{9}
\end{aligned}$$

We now compute the term C (and hence B) analytically. This is possible due to the special structure of the problem, where $p_{\theta}(\mathbf{y} | \mathbf{x})$ is given by the closed form expression (5), with $g(x) = x$. First, by the definition of C we have,

$$\begin{aligned}
C &= \sum_{n=0}^{N-1} \left[|y_n|^2 - 2\Re \left(y_n \sum_{k=0}^{N-1} \mathbb{E}_{q_{\Phi}(\mathbf{x}|\mathbf{y})} \{ \bar{x}_k \} \overline{h_{n-k}} \right) \right. \\
&\quad \left. + \sum_{k,l=0}^{N-1} \mathbb{E}_{q_{\Phi}(\mathbf{x}|\mathbf{y})} \{ x_k \bar{x}_l \} h_{n-k} \overline{h_{n-l}} \right] \tag{10}
\end{aligned}$$

where $\overline{(\cdot)}$ denotes the complex conjugate. Now,

$$\mathbb{E}_{q_{\Phi}(\mathbf{x}|\mathbf{y})} \{ x_k \} = \left(2q_{\Phi,k}^I(\mathbf{y}) - 1 \right) + j \cdot \left(2q_{\Phi,k}^O(\mathbf{y}) - 1 \right) \tag{11}$$

Hence, for the case where $k \neq l$ we have

$$\mathbb{E}_{q_{\Phi}(\mathbf{x}|\mathbf{y})} \{ x_k \bar{x}_l \} = \mathbb{E}_{q_{\Phi}(\mathbf{x}|\mathbf{y})} \{ x_k \} \cdot \mathbb{E}_{q_{\Phi}(\mathbf{x}|\mathbf{y})} \{ \bar{x}_l \} \tag{12}$$

$$\begin{aligned}
&= \left[\left(2q_{\Phi,k}^I(\mathbf{y}) - 1 \right) \left(2q_{\Phi,l}^I(\mathbf{y}) - 1 \right) + \left(2q_{\Phi,k}^O(\mathbf{y}) - 1 \right) \left(2q_{\Phi,l}^O(\mathbf{y}) - 1 \right) \right] + \\
&\quad j \cdot \left[\left(2q_{\Phi,k}^O(\mathbf{y}) - 1 \right) \left(2q_{\Phi,l}^I(\mathbf{y}) - 1 \right) - \left(2q_{\Phi,k}^I(\mathbf{y}) - 1 \right) \left(2q_{\Phi,l}^O(\mathbf{y}) - 1 \right) \right] \tag{13}
\end{aligned}$$

We also have

$$\mathbb{E}_{q_{\Phi}(\mathbf{x}|\mathbf{y})} \{ x_k \bar{x}_k \} = 2 \tag{14}$$

Using (11), (13) and (14) in (10), it is straight-forward to obtain an explicit expression for C . However, in order to compute the third term in the summation over n efficiently, we use the fact that

$$\begin{aligned}
&\sum_{k,l=0}^{N-1} \mathbb{E}_{q_{\Phi}(\mathbf{x}|\mathbf{y})} \{ x_k \bar{x}_l \} h_{n-k} \overline{h_{n-l}} = \\
&\quad \left| \sum_{k=0}^{N-1} \mathbb{E}_{q_{\Phi}(\mathbf{x}|\mathbf{y})} \{ x_k \} h_{n-k} \right|^2 + \\
&\quad \sum_{k=0}^{N-1} |h_{n-k}|^2 \left[2 - \left| \mathbb{E}_{q_{\Phi}(\mathbf{x}|\mathbf{y})} \{ x_k \} \right|^2 \right] \tag{15}
\end{aligned}$$

which follows from (12) and (14). It is now straightforward to use (11), (13), (14) and (15) in (10), and obtain

$$C = \sum_{n=0}^{N-1} \left[|y_n|^2 - 2\alpha_n + \beta_n \right] \quad (16)$$

where

$$\alpha_n = \sum_{k=0}^{N-1} \left\{ y_n^I \cdot \left[h_{n-k}^I \left(2q_{\Phi,k}^I(\mathbf{y}) - 1 \right) - h_{n-k}^O \left(2q_{\Phi,k}^O(\mathbf{y}) - 1 \right) \right] + y_n^O \cdot \left[h_{n-k}^O \left(2q_{\Phi,k}^I(\mathbf{y}) - 1 \right) + h_{n-k}^I \left(2q_{\Phi,k}^O(\mathbf{y}) - 1 \right) \right] \right\} \quad (17)$$

and

$$\begin{aligned} \beta_n = & \left[\sum_{k=0}^{N-1} h_{n-k}^I \left(2q_{\Phi,k}^I(\mathbf{y}) - 1 \right) - h_{n-k}^O \left(2q_{\Phi,k}^O(\mathbf{y}) - 1 \right) \right]^2 \\ & + \left[\sum_{k=0}^{N-1} h_{n-k}^O \left(2q_{\Phi,k}^I(\mathbf{y}) - 1 \right) + h_{n-k}^I \left(2q_{\Phi,k}^O(\mathbf{y}) - 1 \right) \right]^2 \\ & + \sum_{k=0}^{N-1} \left[\left(h_{n-k}^I \right)^2 + \left(h_{n-k}^O \right)^2 \right] \\ & \left[4q_{\Phi,k}^O(\mathbf{y}) + 4q_{\Phi,k}^I(\mathbf{y}) - 4 \left(q_{\Phi,k}^I(\mathbf{y}) \right)^2 - 4 \left(q_{\Phi,k}^O(\mathbf{y}) \right)^2 \right] \end{aligned} \quad (18)$$

Now, to train our VAAE model, we need to minimize $\mathcal{L}(\boldsymbol{\theta}, \Phi, \mathbf{y}) = -A - B$ with respect to $\boldsymbol{\theta} = \{\mathbf{h}, \sigma_w^2\}$ and Φ . We start with the minimization with respect to σ_w^2 . Note that A is independent of σ_w^2 , and B depends on σ_w^2 as described in (9). Hence, by setting the derivative of B with respect to σ_w^2 to zero, we obtain that the optimal value of σ_w^2 is given by $\sigma_w^2 = C/N$. Using this and (7) we see that up to an additive constant (which does not influence the gradients of the learned parameters $\boldsymbol{\theta}, \Phi$), the loss function $\mathcal{L}(\mathbf{h}, \Phi, \mathbf{y})$ (using $\sigma_w^2 = C/N$) for QPSK modulation is given by

$$\mathcal{L}_{\text{QPSK}}(\mathbf{h}, \Phi, \mathbf{y}) = \mathcal{L}(\mathbf{h}, \Phi, \mathbf{y}) = N \log C - \mathcal{H}[q_{\Phi}(\mathbf{x}|\mathbf{y})] \quad (19)$$

where $\mathcal{H}[q_{\Phi}(\mathbf{x}|\mathbf{y})]$ is given in (8), and C is given in (16), (17) and (18). The unknown parameters in our VAAE model are \mathbf{h} and Φ . We estimate these parameters by applying gradient descent based optimization on the loss function $\mathcal{L}(\mathbf{h}, \Phi, \mathbf{y})$ defined in (19).

Recalling the definition of C in (9), we see that our loss function, $\mathcal{L}(\mathbf{h}, \Phi, \mathbf{y})$ defined in (19), consists of a data entropy term, $\mathcal{H}[q_{\Phi}(\mathbf{x}|\mathbf{y})]$, that we wish to maximize (this is reasonable due to the i.i.d assumption of the symbols), and an autoencoder distortion term, $N \log C$, that we wish to minimize.

Our method provides an estimated channel response, \mathbf{h} , as part of the learning process. Note that we do not have to know the exact value of M . Instead, it suffices to have an upper bound on the order of the channel impulse response (or an upper bound on the order of a finite impulse response with which the true channel impulse response can be well approximated). Also note that the decoder network outputs a soft decoding, $\{q_{\Phi,j}^I(\mathbf{y}), q_{\Phi,j}^O(\mathbf{y})\}$, of the transmitted data.

B. BPSK modulation

The derivation above can be degenerated to BPSK modulation, where the transmitted symbols are $x_k \in \{1, -1\}$, representing the bits $c_k \in \{0, 1\}$ (such that $x_k = (-1)^{c_k}$, and the noise is real and Gaussian with expectation zero and variance σ_w^2). In this case, denoting

$$q_{\Phi,j}(\mathbf{y}) \triangleq q_{\Phi,j}(X_j = 1|\mathbf{y}) \quad (20)$$

we have

$$q_{\Phi}(\mathbf{x}|\mathbf{y}) = \prod_{j=0}^{N-1} (q_{\Phi,j}(\mathbf{y}))^{(1+x_j)/2} (1 - q_{\Phi,j}(\mathbf{y}))^{(1-x_j)/2}$$

The loss is

$$\mathcal{L}_{\text{BPSK}}(\mathbf{h}, \Phi, \mathbf{y}) = -A - B$$

where

$$\begin{aligned} A &= \sum_{\mathbf{x}} q_{\Phi}(\mathbf{x}|\mathbf{y}) \cdot (\log p(\mathbf{x}) - \log q_{\Phi}(\mathbf{x}|\mathbf{y})) \\ &= -N \log 2 + \mathcal{H}[q_{\Phi}(\mathbf{x}|\mathbf{y})] \end{aligned} \quad (21)$$

and

$$\begin{aligned} \mathcal{H}[q_{\Phi}(\mathbf{x}|\mathbf{y})] &= \mathcal{H}\left[\prod_{j=0}^{N-1} q_{\Phi,j}(x_j|\mathbf{y})\right] = \sum_{j=0}^{N-1} \mathcal{H}[q_{\Phi,j}(x_j|\mathbf{y})] \\ &= -\sum_{j=0}^{N-1} [q_{\Phi,j}(\mathbf{y}) \log q_{\Phi,j}(\mathbf{y}) + (1 - q_{\Phi,j}(\mathbf{y})) \log (1 - q_{\Phi,j}(\mathbf{y}))] \end{aligned} \quad (22)$$

Instead of the QPSK loss, Eq. (19), we now have

$$\mathcal{L}_{\text{BPSK}}(\mathbf{h}, \Phi, \mathbf{y}) = \frac{N}{2} \log C - \mathcal{H}[q_{\Phi}(\mathbf{x}|\mathbf{y})] \quad (23)$$

for

$$\begin{aligned} C &\triangleq \mathbb{E}_{q_{\Phi}(\mathbf{x}|\mathbf{y})} [\|\mathbf{y} - \mathbf{x} * \mathbf{h}\|^2] \\ &= \sum_{n=0}^{N-1} \left\{ (y_n)^2 - 2y_n \sum_{k=0}^{N-1} (2q_{\Phi,k}(\mathbf{y}) - 1) h_{n-k} \right. \\ &\quad \left. + \left[\sum_{k=0}^{N-1} (2q_{\Phi,k}(\mathbf{y}) - 1) h_{n-k} \right]^2 \right. \\ &\quad \left. + \sum_{k=0}^{N-1} (h_{n-k})^2 [4q_{\Phi,k}(\mathbf{y}) - 4(q_{\Phi,k}(\mathbf{y}))^2] \right\} \end{aligned} \quad (24)$$

Our decoder network for BPSK signaling, implementing $\{q_{\Phi,j}(\mathbf{y})\}$, is depicted in Fig. 4. Unlike the QPSK case, we now use standard real one dimensional convolutional layers.

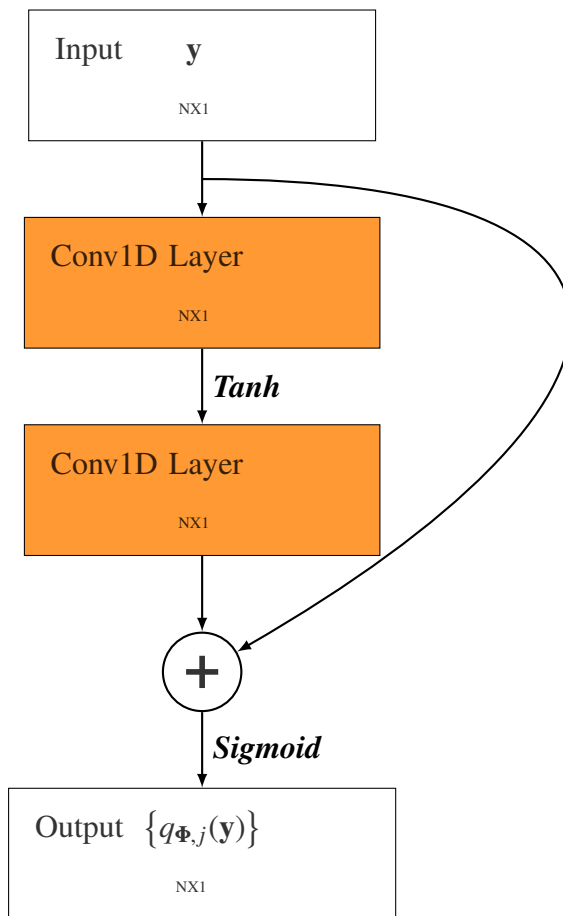


Fig. 4: Our equalizer's architecture for BPSK communication.

IV. PROPOSED METHOD FOR A NOISY NONLINEAR ISI CHANNEL

Some authors have considered the nonlinear channel equalization problem, but only under a supervised learning setup, which requires pilot signals for training the equalizer, [25]–[29]. We now consider the extension of our unsupervised blind VAAE to noisy nonlinear ISI channels. The channel model is described by (1) and (2) in Section II with an unknown, possibly nonlinear, function $g(\cdot)$ (also shown in Fig. 1) in addition to the other unknown channel parameters. Throughout this section we assume BPSK modulation, but the same derivation can be used for QPSK modulation.

Since the nonlinear function $g(\cdot)$ is unknown and needs to be learned, we use an encoder neural network in addition to the decoder neural network that we had in the linear channel case. The encoder neural network has input \mathbf{x} and output $G(\mathbf{x}, \boldsymbol{\theta})$ where $\boldsymbol{\theta}$ is the neural network's parameter vector. The vector $\boldsymbol{\theta}$ includes both the unknown ISI channel response, \mathbf{h} , and the neural network parameters, $\boldsymbol{\psi}$, used to model the nonlinearity $g(\cdot)$, i.e., $\boldsymbol{\theta} = (\mathbf{h}, \boldsymbol{\psi})$. The encoder $G(\mathbf{x}, \boldsymbol{\theta})$ needs to implement (approximate) the function $g(\mathbf{x} * \mathbf{h})$, i.e.,

$$\mathbf{G}(\mathbf{x}, \boldsymbol{\theta}) \approx g(\mathbf{x} * \mathbf{h})$$

The encoder network we use is described in Figs. 5-6 and Table I. As can be seen in Fig. 5, the encoder

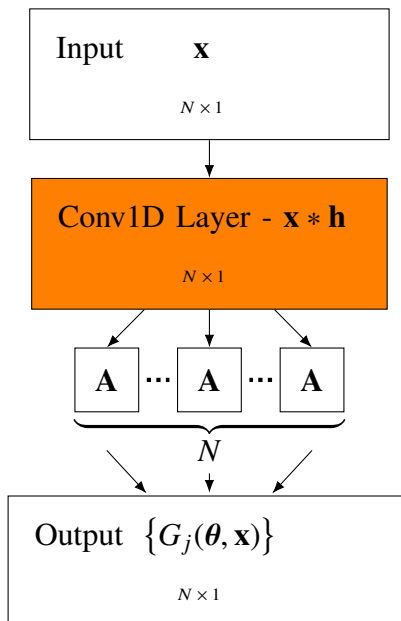


Fig. 5: Our new encoder architecture using a neural network A block shown in Fig. 6.

TABLE I: The Encoder's Fully Connected Neural Network A Layout

| Layer | Output dimensions |
|---------|-------------------|
| Input | 1 |
| FC/ReLU | 5 |
| Dropout | 5 |
| FC/ReLU | 5 |
| Dropout | 5 |
| Linear | 1 |

network first applies the convolution with \mathbf{h} using a convolutional layer. We then implement the function $g(\cdot)$ using the neural network A, shown in Fig. 6. The neural network A is applied component-wise on the results of the convolution with \mathbf{h} . It uses a fully connected (FC) architecture as described in Fig. 6 and Table I, including ReLU activation functions, dropout layers [40] and a linear output layer.

Repeating the derivation in Section III-B for the nonlinear case, the new loss function $\mathcal{L}_{\text{BPSK}}^{\text{NL}}(\boldsymbol{\theta}, \boldsymbol{\Phi}, \mathbf{y})$ is given by the same expression (23), i.e.,

$$\mathcal{L}_{\text{BPSK}}^{\text{NL}}(\boldsymbol{\theta}, \boldsymbol{\Phi}, \mathbf{y}) = \frac{N}{2} \log C_{\text{NL}} - \mathcal{H}[q_{\boldsymbol{\Phi}}(\mathbf{x}|\mathbf{y})] \quad (25)$$

where $\mathcal{H}[q_{\boldsymbol{\Phi}}(\mathbf{x}|\mathbf{y})]$ is given by (22) for $q_{\boldsymbol{\Phi},j}(\mathbf{y})$ defined by (20). However, unlike the analytic computation of C in Section III for linear channels, C_{NL} , which is defined by

$$C_{\text{NL}} \triangleq \mathbb{E}_{q_{\boldsymbol{\Phi}}(\mathbf{x}|\mathbf{y})} \left[\|\mathbf{y} - g(\mathbf{x} * \mathbf{h})\|^2 \right]$$

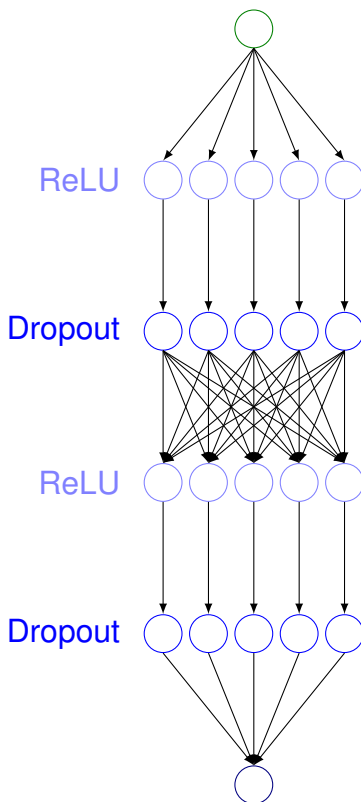


Fig. 6: The neural network A in Fig. 5.

$$\begin{aligned}
&= \mathbb{E}_{q_{\Phi}(\mathbf{x}|\mathbf{y})} \left[\|\mathbf{y} - \mathbf{G}(\mathbf{x}, \boldsymbol{\theta})\|^2 \right] \\
&= \mathbb{E}_{q_{\Phi}(\mathbf{x}|\mathbf{y})} \left\{ \sum_{n=0}^{N-1} [y_n - G_n(\mathbf{x}, \boldsymbol{\theta})]^2 \right\} \tag{26}
\end{aligned}$$

($G_n(\cdot)$ is the n -th output cell of the neural network) cannot be computed analytically. Our decoder network, implementing $q_{\Phi,j}(\mathbf{y})$, is the same as in Section III-B (Fig. 4). Hence, we now have two neural networks, an encoder neural network implementing $\mathbf{G}(\mathbf{x}, \boldsymbol{\theta})$, and a decoder neural network implementing $q_{\Phi}(\mathbf{x}|\mathbf{y})$. The two neural networks are trained jointly using a gradient descent approach. Hence, we need to compute the gradient of $\mathcal{L}_{\text{BPSK}}^{\text{NL}}(\boldsymbol{\theta}, \Phi, \mathbf{y})$ with respect to $\boldsymbol{\theta}$ and Φ . By (25) and (26) we have

$$\nabla_{\boldsymbol{\theta}} \mathcal{L}_{\text{BPSK}}^{\text{NL}}(\boldsymbol{\theta}, \Phi, \mathbf{y}) = \frac{N}{2} \nabla_{\boldsymbol{\theta}} \log \mathbb{E}_{q_{\Phi}(\mathbf{x}|\mathbf{y})} \left\{ \sum_{n=0}^{N-1} [y_n - G_n(\mathbf{x}, \boldsymbol{\theta})]^2 \right\} \tag{27}$$

$$\nabla_{\Phi} \mathcal{L}_{\text{BPSK}}^{\text{NL}}(\boldsymbol{\theta}, \Phi, \mathbf{y}) = \frac{N}{2} \nabla_{\Phi} \log \mathbb{E}_{q_{\Phi}(\mathbf{x}|\mathbf{y})} \left\{ \sum_{n=0}^{N-1} [y_n - G_n(\mathbf{x}, \boldsymbol{\theta})]^2 \right\} - \nabla_{\Phi} \mathcal{H}[q_{\Phi}(\mathbf{x}|\mathbf{y})] \tag{28}$$

The second term in the right hand side (RHS) of (28) can be easily computed from (22) (the derivative of $q_{\Phi,j}(\mathbf{y})$ with respect to Φ is obtained by the backpropagation algorithm applied to the decoder neural network). Following the common approach [31], [41], the gradient with respect to $\boldsymbol{\theta}$ in (27) can be well

approximated using

$$\nabla_{\theta} \mathcal{L}_{\text{BPSK}}^{\text{NL}}(\theta, \Phi, \mathbf{y}) \approx \frac{N}{2} \nabla_{\theta} \log \left\{ \sum_{n=0}^{N-1} [y_n - G_n(\hat{\mathbf{x}}, \theta)]^2 \right\}$$

where $\hat{\mathbf{x}}$ is obtained by sampling using the Bernoulli distribution with probabilities given by the output of the decoder neural network that implements $\{q_{\Phi,j}(\mathbf{y})\}$, i.e., we set $\hat{x}_j = 1$ ($\hat{x}_j = -1$, respectively) with probability $q_{\Phi,j}(\mathbf{y})$ ($1 - q_{\Phi,j}(\mathbf{y})$).

However, it is more difficult to obtain a reliable estimate to the first term in the RHS of (28). When \mathbf{x} in the model is continuous (e.g., a Gaussian random variable), the reparameterization trick can be used [31]. For discrete \mathbf{x} (as in our problem), the reparameterization trick cannot be applied. Instead, various approximation schemes to the gradient have been suggested, e.g., [41], [42]. In [43], [44] the gradient is approximated using continuous relaxations of discrete distributions. This approximation was shown to possess a favorable trade-off between estimation quality, computational complexity and sample efficiency. Hence it was adopted in our work.

The method in [43], [44] is based on a continuous relaxation of the Gumbel-Max trick [45], [46], which allows us to sample from a categorical distribution (in our case this is the Bernoulli distribution with probabilities $(q_{\Phi,j}(\mathbf{y}), 1 - q_{\Phi,j}(\mathbf{y}))$). Denote by $U(0, 1)$ the standard uniform distribution. We repeat the following procedure for $j = 0, 1, \dots, N - 1$: We first sample $u_{j,k} \sim U(0, 1)$, and set $g_{j,k} = -\log(-\log u_{j,k})$ for $k = 1, 2$. By definition, $g_{j,1}$ and $g_{j,2}$ are said to be Gumbel(0, 1) distributed. We now define, for $j = 0, 1, \dots, N - 1$,

$$\begin{aligned} \hat{c}_j &\triangleq \frac{\exp((\log q_{\Phi,j}(\mathbf{y}) + g_{j,1})/\tau)}{\exp((\log q_{\Phi,j}(\mathbf{y}) + g_{j,1})/\tau) + \exp((\log(1 - q_{\Phi,j}(\mathbf{y})) + g_{j,2})/\tau)} \\ \hat{x}_j &\triangleq 2\hat{c}_j - 1 \end{aligned} \quad (29)$$

where $\tau > 0$ is some parameter (temperature). It can be shown [43], [44], that for $\tau \rightarrow 0$, the resulting $\hat{\mathbf{x}}$ is a sample from the distribution $q_{\Phi}(\mathbf{x}|\mathbf{y})$ (\hat{c}_j is the sampled soft bit value, and \hat{x}_j is the corresponding sampled soft BPSK modulated symbol). Our estimate to the first term in the RHS of (28) is then

$$\frac{N}{2} \nabla_{\Phi} \log \sum_{n=0}^{N-1} [y_n - G_n(\hat{\mathbf{x}}, \theta)]^2$$

We set $\tau > 0$ to keep \hat{x}_j , defined in (29), smooth and differentiable with respect to Φ . In our simulations we initialize the temperature to $\tau = 5$ and set it to be trainable as recommended in [43], [44].

V. EXTENSION TO LDPC CODED COMMUNICATION

In order to enable reliable communications at rates close to channel capacity, an error correcting code needs to be incorporated. In this section we assume the availability of only the channel observations corresponding to a single transmitted codeword, without knowing the channel parameters and without

using pilot signals that reduce the communication rate. The goal is to reconstruct the transmitted message from this data alone in an unsupervised way. It is useful for a fast changing communication (e.g., wireless) environments.

Throughout the section we assume a noisy linear ISI channel and BPSK modulation. However, the same derivation can be applied to a noisy nonlinear ISI channel. In the simulations section we report results for both the linear and nonlinear cases under BPSK modulation. The results can also be easily extended to other modulation schemes (e.g., QPSK). We discuss the case where the transmitted data, \mathbf{x} , is a BPSK modulated codeword, \mathbf{c} (i.e. $x_k = (-1)^{c_k}$), of a sparse graph-based code. For concreteness, in this paper we assume an LDPC code [47]. However, our methods can be used for other linear sparse graphical codes such as turbo codes, to which BP decoding can be applied.

A binary LDPC code, \mathcal{C} , is a binary linear code that can be described by a sparse binary parity check matrix H of dimensions $J \times N$, such that $\mathcal{C} = \{\mathbf{c} : H\mathbf{c} = \mathbf{0}\}$. The blocklength of the code is N , and the code rate is at least $(N - J)/N$ (due to a possible linear dependence between the rows of H). The matrix H can also be represented by a *Tanner graph*, \mathcal{G} , [48] which is a sparse bipartite graph, with N left nodes, \mathcal{I} , also called variable nodes, and J right nodes, \mathcal{J} , also called parity check nodes. A variable node $i \in \mathcal{I}$ (parity check node $j \in \mathcal{J}$, respectively), can only connect to parity check (variable) nodes. We denote this set of neighbor nodes by \mathcal{N}_i (\mathcal{N}_j , respectively). An edge connects the parity check node $j \in \mathcal{J}$ and the variable node $l \in \mathcal{I}$ if and only if $H_{j,l} = 1$. LDPC codes can be efficiently decoded using Gallager's probabilistic decoding algorithm, also known as the sum-product or BP algorithm. This algorithm is a message passing algorithm over edges in the Tanner graph [48].

We describe two methods for enhancing the operation of our VAEE when \mathbf{x} is a BPSK modulated LDPC codeword. In section V-A we add a loss term that penalizes the soft decoding based on the estimated probabilities that the check nodes in the Tanner graph are not satisfied. In section V-B we suggest a decoding scheme that applies the VAEE followed by the BP decoding algorithm iteratively similarly to [8]. In our experiments we observed that both methods were useful to improve decoding, and the best results were obtained by using both simultaneously (results are provided below in the simulations section).

A. Augmenting the loss using Gallager's lemma

In [47, Lemma 1], Gallager proved the following. Consider m statistically independent bits, where the l 'th bit is 1 with probability P_l and 0 with probability $1 - P_l$. Then the probability that an even number of bits are 1 is

$$\frac{1 + \prod_{l=1}^m (1 - 2P_l)}{2}$$

Recall that $q_{\Phi,l}(\mathbf{y})$ ($1 - q_{\Phi,l}(\mathbf{y})$, respectively) is an estimate to the probability that $x_l = 1$ ($x_l = -1$), corresponding to $c_l = 0$ ($c_l = 1$). Hence, by [47, Lemma 1], for any parity check node, $j \in \mathcal{J}$, the

probability that the check node is satisfied, i.e., an even number of variable nodes $l \in \mathcal{N}_j$ satisfy $c_l = 1$, can be estimated by

$$\frac{1 + \prod_{l \in \mathcal{N}_j} (2q_{\Phi,l}(\mathbf{y}) - 1)}{2}$$

Now, for a valid codeword $\mathbf{c} \in C$, all check nodes are satisfied. Hence we request a low value to the following *Gallager loss* defined by,

$$\begin{aligned} \mathcal{L}_G(\Phi, \mathbf{y}) &= -\log \prod_{j \in \mathcal{J}} \frac{1 + \prod_{l \in \mathcal{N}_j} (2q_{\Phi,l}(\mathbf{y}) - 1)}{2} \\ &= -\sum_{j \in \mathcal{J}} \log \frac{1 + \prod_{l \in \mathcal{N}_j} (2q_{\Phi,l}(\mathbf{y}) - 1)}{2} \end{aligned}$$

Instead of $\mathcal{L}_{\text{BPSK}}(\mathbf{h}, \Phi, \mathbf{y})$ in (23), we thus propose the following augmented loss for the coded data case

$$\mathcal{L}_{\text{BPSK}}^G(\mathbf{h}, \Phi, \mathbf{y}) = \lambda \cdot \mathcal{L}_{\text{BPSK}}(\mathbf{h}, \Phi, \mathbf{y}) + (1 - \lambda) \cdot \mathcal{L}_G(\Phi, \mathbf{y}) \quad (30)$$

where $\lambda \in [0, 1]$ is a hyper-parameter determining how much weight is assigned to each component of the total loss. Note that for $\lambda = 0$ our loss function is just $\mathcal{L}_G(\Phi, \mathbf{y})$, and the decoder can produce the trivial solution, $q_{\Phi,l}(\mathbf{y}) = 1$ for all l , corresponding to the zero codeword. Hence, we must set $\lambda > 0$.

Our Gallager loss, $\mathcal{L}_G(\Phi, \mathbf{y})$, is similar to the *syndrome loss* introduced in [49]. However, in [49] the syndrome loss is used to improve the training of a neural message passing decoder, while in our work the Gallager loss is used for blind channel equalization of coded data. In addition, our a loss is a likelihood based score.

B. Iterative VAE Equalization and BP decoding

We now extend the VAEE to a turbo VAEE algorithm that applies VAEE and BP decoding iteratively, similarly to the turbo equalization algorithm [34], [35]. We start the first iteration of the turbo VAEE algorithm by applying the VAEE. The prior probability of the transmitted binary data, \mathbf{x} (where $x_k \in \{1, -1\}$), is then uniform

$$p(\mathbf{x}) = p^{(1)}(\mathbf{x}) = \prod_j p_j^{(1)}(x_j) = 2^{-N} \quad (31)$$

as in (3). The output of the VAEE (with or without the Gallager loss term that incorporates some coding information) are the probabilities $\{q_{\Phi,j}(\mathbf{y}) = q_{\Phi,j}(X_j = 1 | \mathbf{y})\}$. We then apply the BP algorithm using these probabilities, produced by the VAEE, as uncoded data from the channel. The corresponding uncoded log-likelihood ratios (LLRs) at the input to the BP algorithm are

$$\text{LLR}_j^{(1)} = \log \frac{q_{\Phi}(X_j = 1 | \mathbf{y})}{q_{\Phi}(X_j = -1 | \mathbf{y})} = \log \frac{q_{\Phi,j}(\mathbf{y})}{1 - q_{\Phi,j}(\mathbf{y})}$$

for $j = 0, 1, \dots, N-1$. The outputs of the BP are soft decoding LLRs of the transmitted codeword, denoted by

$$\overline{\text{LLR}}_j^{(1)} = \log \frac{\overline{p}_j^{(1)}(X_j = 1)}{\overline{p}_j^{(1)}(X_j = -1)} \quad (32)$$

where $\overline{p}_j^{(1)}(X_j = x_j) = \overline{p}_j^{(1)}(x_j)$ are the probabilities obtained by the BP algorithm. Note that according to the principles of message passing algorithms [48], for each j the final marginalization used to obtain $\overline{\text{LLR}}_j^{(1)}$ does not include the input channel LLR message $\text{LLR}_j^{(1)}$. By (32), $\overline{p}_j^{(1)}(X_j = 1)$ can be extracted from $\overline{\text{LLR}}_j^{(1)}$ using

$$\overline{p}_j^{(1)}(X_j = 1) = \left(1 + e^{-\overline{\text{LLR}}_j^{(1)}}\right)^{-1} \quad (33)$$

We now move on to the second turbo VAEE iteration by applying VAEE using

$$p(\mathbf{x}) = p^{(2)}(\mathbf{x}) = \prod_j \overline{p}_j^{(1)}(x_j) \quad (34)$$

as prior probabilities of the transmitted data, \mathbf{x} . Recall that the VAEE was derived under the assumption of uniform $p(\mathbf{x})$ as in (3) and (31). Hence, we need to generalize the algorithm to the case where the prior probability is given in (34). This is easy, however, since the only change in the VAEE training is in the computation of the term A , which was previously calculated using (21), and is now computed as follows,

$$\begin{aligned} A &= \sum_{\mathbf{x}} q_{\Phi}(\mathbf{x}|\mathbf{y}) (\log p(\mathbf{x}) - \log q_{\Phi}(\mathbf{x}|\mathbf{y})) \\ &= \sum_{\mathbf{x}} q_{\Phi}(\mathbf{x}|\mathbf{y}) \sum_j \log p_j(x_j) + \mathcal{H}[q_{\Phi}(\mathbf{x}|\mathbf{y})] \\ &= \sum_{\mathbf{x}} \prod_{l=0}^{N-1} q_{\Phi}(x_l|\mathbf{y}) \sum_j \log p_j(x_j) + \mathcal{H}[q_{\Phi}(\mathbf{x}|\mathbf{y})] \\ &= \sum_j \sum_{x_j} q_{\Phi}(x_j|\mathbf{y}) \log p_j(x_j) + \mathcal{H}[q_{\Phi}(\mathbf{x}|\mathbf{y})] \\ &= \sum_j \sum_{x \in \{-1,1\}} q_{\Phi,j}(x|\mathbf{y}) \log p_j(x) + \mathcal{H}[q_{\Phi}(\mathbf{x}|\mathbf{y})] \end{aligned}$$

The corrected loss to be minimized instead of (23) is thus

$$\mathcal{L}'_{\text{BPSK}}(\mathbf{h}, \Phi, \mathbf{y}) = \frac{N}{2} \log C - \mathcal{H}[q_{\Phi}(\mathbf{x}|\mathbf{y})] - \sum_j \sum_{x \in \{-1,1\}} q_{\Phi,j}(x|\mathbf{y}) \log p_j(x) \quad (35)$$

where C is given in (24) (the Gallager loss \mathcal{L}_G can also be used by adding it to the above loss term).

The same procedure is repeated in the other decoding iterations. In general, in the first stage of the l -th iteration ($l = 1, 2, \dots$), our proposed turbo VAEE applies the VAEE, by minimizing (35) (possibly with the addition of the Gallager loss, \mathcal{L}_G , as in (30)) using

$$p_j(x) = p_j^{(l)}(x) = \overline{p}_j^{(l-1)}(x) \quad (36)$$

for $j = 0, 1, \dots, N - 1$ and $x \in \{1, -1\}$ as input (for initialization, $l = 1$, we use $p_j(x) = p_j^{(1)}(x) = 1/2$ as was described above). The VAAE produces the probabilities $q_{\Phi,j}(\mathbf{y}) = q_{\Phi,j}(X_j = 1|\mathbf{y})$. Then, in the second stage of the l -th iteration, we apply the BP algorithm, using $q_{\Phi,j}(\mathbf{y})$ as uncoded probabilities from the channel. The BP algorithm produces the probabilities $\bar{p}_j^{(l)}(x)$, $x \in \{1, -1\}$ as in the first iteration: $\overline{\text{LLR}}_j^{(l)}$ is obtained from variable node final marginalization, by summing all incoming final LLR messages to variable node j in the Tanner graph, except for the input channel LLR message, $\text{LLR}_j^{(l)} = \log \frac{q_{\Phi,j}(\mathbf{y})}{1 - q_{\Phi,j}(\mathbf{y})}$, and then $\bar{p}_j^{(l)}(X_j = 1) = \left(1 + e^{-\overline{\text{LLR}}_j^{(l)}}\right)^{-1}$ as in (33). These probabilities are subsequently used as input to the next $(l + 1)$ iteration of the VAAE.

Due to the presence of short cycles in the code Tanner graph, we found it useful to weaken the prior probabilities used in the beginning of each iteration by modifying (36) to

$$p_j(x) = p_j^{(l)}(x) = \alpha \bar{p}_j^{(l-1)}(x) + (1 - \alpha) \frac{1}{2} \quad (37)$$

for $j = 0, 1, \dots, N - 1$ and $x \in \{1, -1\}$, where α is some hyper-parameter.

An high-level system scheme is shown in Fig. 7.

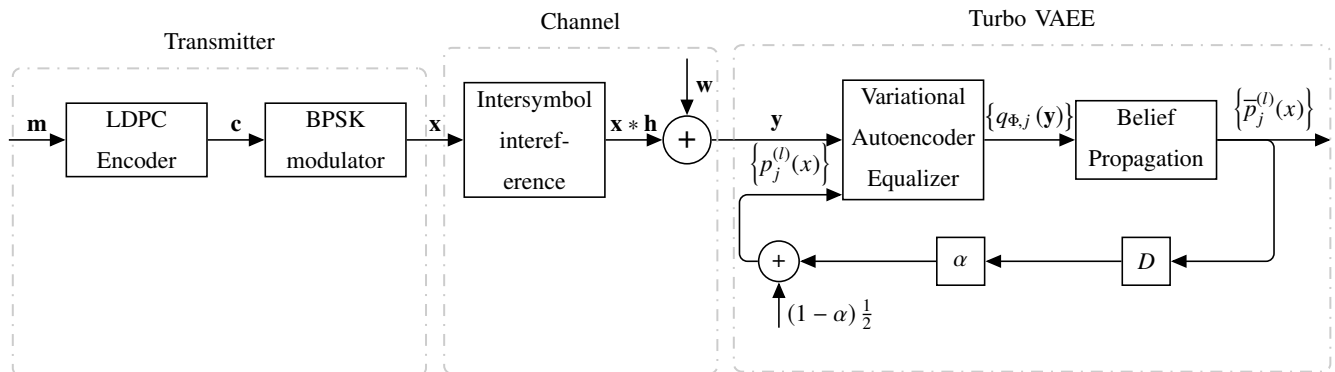


Fig. 7: Our proposed turbo VAAE which consists of iterative VAAE and BP decoding. D is a delay element.

VI. SIMULATION RESULTS

In our derivation above we assumed that the input signal $\{x_k\}$ is causal. However, if we are considering a sampled block $\mathbf{y} = (y_0, y_1, \dots, y_{N-1})$ of N measurements of the signal starting at some arbitrary time, then the above causality assumption on \mathbf{x} does not hold. Nevertheless, the edge effect decays as N increases. The causality assumption is equivalent to $M - 1$ zero-padding of $\mathbf{x} = (x_0, x_1, \dots, x_{N-1})$ on the left. Alternatively (supposing odd M for simplicity), we can assume that $\mathbf{h} = (h_{-(M-1)/2}, \dots, h_0, \dots, h_{(M-1)/2})$. Accordingly, we assume zero-padding of $\mathbf{x} = (x_0, x_1, \dots, x_{N-1})$ by $(M - 1)/2$ both on the left and on the right, and the given measurements vector $\mathbf{y} = (y_0, y_1, \dots, y_{N-1})$ is the result of the channel model (2). We used

this second approach in our experiments with uncoded data, although the performance was similar to the performance of the first approach.

For the experiments with coded data we assumed that the transmitted BPSK modulated codeword $\mathbf{x} = (x_0, x_1, \dots, x_{N-1})$ is zero padded on the left and on the right. The filter $\mathbf{h} = (h_0, h_1, \dots, h_{M-1})$ is a causal size M impulse response. The channel measurements are $\mathbf{y} = (y_0, y_1, \dots, y_{N+M-2})$ ($N + M - 1$ measurements). The same conditions were used for the baseline methods that we compared with.

We implemented our VAAE algorithms using the Tensorflow framework [50] which provides automatic differentiation of the loss function. For the LDPC infrastructure, we used the software toolbox in [51]. For the turbo operation mode, we used the BP algorithm implemented in [8].

A. Linear channels, uncoded data

We start by reporting results for noisy linear ISI channels under QPSK modulation, without using coding information. Our algorithm was compared with the adaptive CMA [52], and with the neural network CMA (NNCMA) [15] blind equalization algorithms. In addition, we compared the performance to the adaptive linear MMSE [33] non-blind equalizer that observes the actual transmitted sequence. The baseline algorithms use a single pass over the data for training. In order to improve performance, they were modified to have sufficiently many passes over the data. In our first experiments in this subsection, reported in Figs. 8, 9 and 10, we used the Adam optimization algorithm [53] to minimize our loss function. For all experiments in the uncoded case, and all blind equalization methods, we note that one can recover the transmitted bits only up to some unknown delay and rotation of the constellation, which for QPSK means that we need to examine four different possible rotations ($0^\circ, 90^\circ, 180^\circ, 270^\circ$). The results presented in the following experiments were obtained by averaging over 20 independent training data sequences. For each training data sequence, we used $K = 10,000$ test data symbols to calculate the symbol error rate (SER), taking into account all possible rotations and delays.

In all our experiments, we used the same FCN decoder architecture in Fig. 3, with a filter with five complex coefficients in the first layer, and a filter with two complex coefficients in the second layer. Hence, the total number of free parameters in the model was only $M + 15$ (M channel impulse response parameters in the encoder, 1 parameter representing the noise variance, and 14 ($2 \times (5 + 2)$) real parameters in the FCN decoder).

In our first set of experiments, we compared our model to the baseline algorithms at various noise

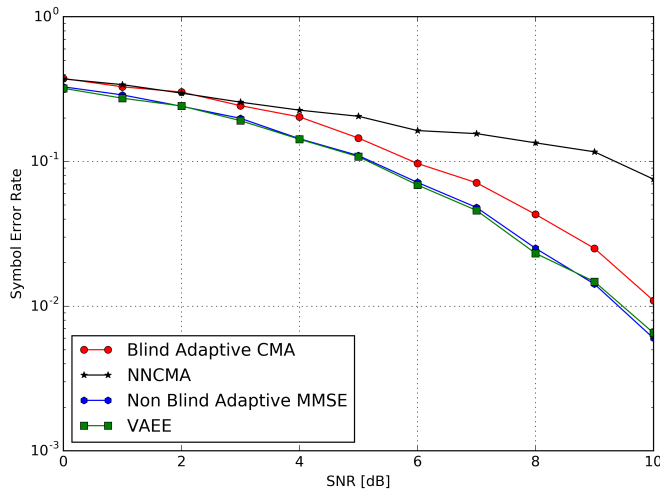


Fig. 8: SER vs. SNR for the equalization algorithms. The channel is \mathbf{h}_1 .

levels, using the following non-minimum phase channels taken from [54], [55]

$$\begin{aligned} \mathbf{h}_1 &= [0.0545 + 0.05j, 0.2832 - 0.11971j, -0.7676 + 0.2788j, \\ &\quad -0.0641 - 0.0576j, 0.0466 - 0.02275j] \\ \mathbf{h}_2 &= [0.0554 + 0.0165j, -1.3449 - 0.4523j, \\ &\quad 1.0067 + 1.1524j, 0.3476 + 0.3153j] \end{aligned}$$

We generated $L = 2000$ QPSK random symbols as the training sequence. Then we applied convolution with the channel impulse response, and added white Gaussian noise at a signal to noise ratio (SNR) in the range 0dB – 10dB. The SNR is defined by $\text{SNR} \triangleq 20 \log_{10} (\|\mathbf{x} * \mathbf{h}\| / \|\mathbf{w}\|)$. To train the model, for each update step, we sampled from the training set a mini-batch of a single sub-sequence of length $N = 128$. Figs. 8 and 9 present SER results for \mathbf{h}_1 and \mathbf{h}_2 respectively. As can be seen, the new VAEE significantly outperforms the baseline blind equalizers, and is quite close to the performance of the non-blind adaptive linear MMSE equalizer.

In our following experiment, we compared the SER of the equalization algorithms as the number of training symbols varied from $L = 50$ to $L = 500,000$. For each update step we sampled from the training set a mini-batch of a single sub-sequence of length $N = \min(128, L)$. We used the channel impulse response \mathbf{h}_1 above. Fig. 10 presents the results for SNR=10dB. Again, the new VAEE algorithm significantly outperforms the baseline blind equalization algorithms. The results show that the VAEE enables faster channel acquisition compared to the other blind equalization algorithms.

Further experiments for uncoded data are reported in [30].

For maintaining good performance but faster convergence time, we re-ran simulations from [30] using a variety of gradient descent-based optimizers. In Fig. 11 we report on the number of parameter updates

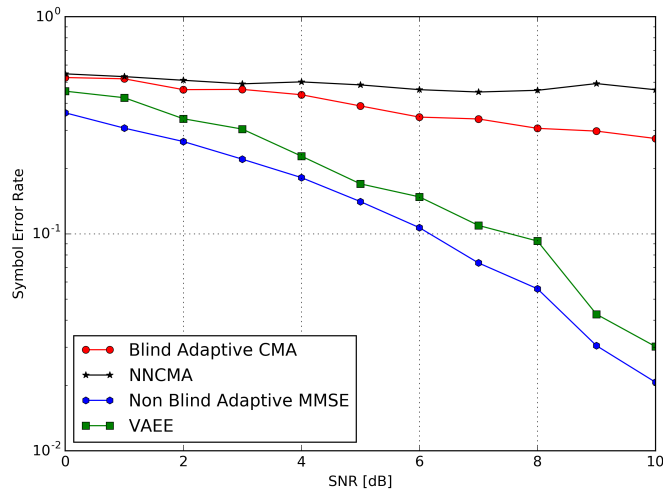


Fig. 9: SER vs. SNR for the equalization algorithms. The channel is \mathbf{h}_2 .

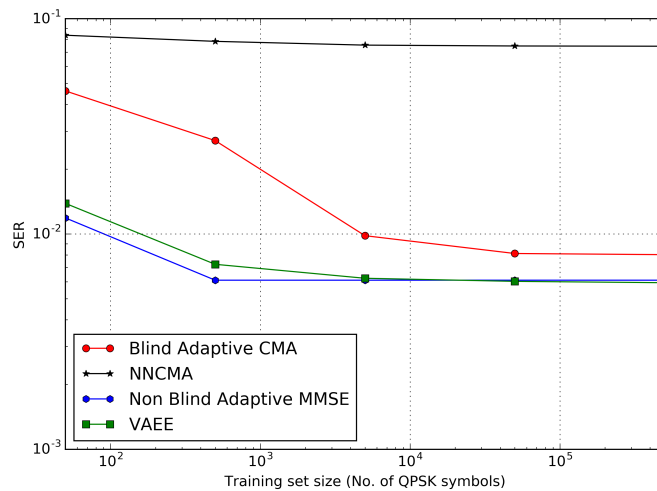


Fig. 10: SER vs. number of training symbols for the equalization algorithms. SNR = 10dB. The channel is \mathbf{h}_1 .

required for convergence of the VAEE algorithm when using the channel \mathbf{h}_1 . To train the model, we sampled a mini-batch of a single sub-sequence of length $N \in \{10, 128\}$ out of the given training symbols. Then we let the algorithm train until convergence was achieved. As presented in Fig. 11, the AMSGrad optimizer [56] leads to a significant speedup in the training of our model compared to the Adam algorithm [53]. The BER and SER performance did not change much between optimizers. Thus, we used the AMSGrad optimizer in our subsequent simulations.

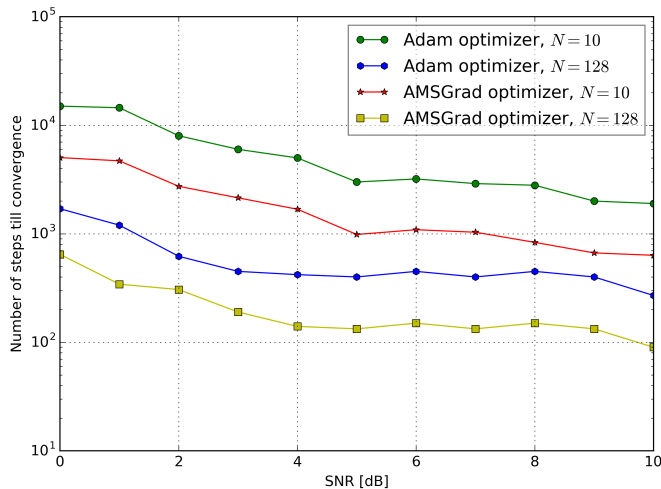


Fig. 11: Number of parameter updates vs. SNR for different N . The channel is \mathbf{h}_1 .

B. Linear channels, coded data

In all our experiments with coded data we assume the availability of only the channel observations corresponding to a single transmitted LDPC codeword. As explained above, our goal is to reconstruct the transmitted message from this data alone without knowing the channel parameters. As an upper bound on the performance, we compared our results to the non-blind turbo equalization algorithm [34], [35] which knows the true channel. This algorithm applies the BCJR algorithm [24] and the BP algorithm iteratively.

We then implemented and compared our algorithm to the (blind) EM algorithm [23] for a noisy linear ISI channel, taking into account the coding information similarly to [22]. In every iteration, this *turbo EM* algorithm re-estimates the ISI channel impulse response and the noise variance. It applies the generalized BCJR algorithm [20] and the BP algorithm iteratively as in the turbo equalization algorithm. As explained in [20], the accurate implementation of the EM requires the computation of the posterior joint expectation $\mathbb{E}[x_i, x_j | \mathbf{y}]$ of two transmitted symbols. In the approximated EM algorithm for a noisy ISI channel proposed in [19], the approximation $\mathbb{E}[x_i x_j | \mathbf{y}] \approx \mathbb{E}[x_i | \mathbf{y}] \cdot \mathbb{E}[x_j | \mathbf{y}]$ is used. Under this approximation, the standard BCJR algorithm is sufficient to implement EM estimation. To improve results, a generalized BCJR is derived in [20] to compute $\mathbb{E}[x_i, x_j | \mathbf{y}]$ accurately. We have also implemented and evaluated channel estimation with the least squares method as described in [16]. These results are not shown since in all our experiments the EM algorithm outperformed the least squares estimation method. As noted above, the turbo equalization algorithm is channel informed, i.e., it knows the true ISI channel impulse response and noise variance. On the other hand, our turbo VAAE algorithm and the turbo EM algorithm are blind. They perform unsupervised joint estimation of the channel coefficients, noise variance and the transmitted codeword.

For each experiment we show the Shannon threshold SNR for which channel capacity is equal to the

code rate used. The capacity of the noisy ISI channel was computed using the water-filling algorithm [57] under a power constraint of 1 corresponding to the input power under BPSK modulation.

In all our experiments with coded data, we used the same FCN decoder architecture in Fig. 4. We used a filter with 10 coefficients in the first layer, and a filter with 5 coefficients in the second layer. Hence, the total number of free parameters in the model was $M + 16$ (M parameters for the channel impulse response, 1 parameter for the the channel noise variance, and 15 parameters for the FCN decoder). In the turbo VAAE experiments we first applied standalone VAAE for I iterations, and only then started turbo mode where we apply T external iterations, each consisting of one VAAE iteration and B BP iterations. The values of the hyper-parameters used are summarized in Table II.

TABLE II: Values of the hyper-parameters.

| Variable | Definition | Value |
|-----------|--|--------------------|
| T | Total number of training iterations | 60 |
| lr | Learning rate for VAAE training | $12 \cdot 10^{-2}$ |
| λ | Weight in (30) | 0.55 |
| α | Coefficient in (37) | 0.2 |
| B | Number of BP iterations after each VAAE iteration | 15 |
| I | Number of VAAE iterations before applying turbo mode | 40 |

The results presented in the following experiments were obtained by averaging over 20 independent transmitted codewords. Each chosen codeword was transmitted several times, each time with a different noise sequence realization. The number of noise sequences used was determined based on the bit error rate (BER), in order to obtain stable BER estimates. The BER of the decoded codeword is defined by

$$\text{BER} \triangleq \mathbb{E} \left[\mathbb{1} \left(\hat{b} \neq b \right) \right] = \frac{1}{N} \sum_b \mathbb{1} \left(\hat{b} \neq b \right)$$

where N is the code blocklength, b is a BPSK coded symbol and \hat{b} is the corresponding decoded symbol. We evaluated the various decoding algorithms at various noise levels, using two LDPC codes from the Wimax IEEE 802.16e standard. The parity check matrices are taken from [51]. The first code has blocklength $N_1 = 576$ and the second has blocklength $N_2 = 2304$. The rate of both codes is $3/4$. The following causal non-minimum phase channel impulse responses were used to simulate the ISI,

$$\tilde{\mathbf{h}}_1 = [0.2, 0.9, 0.3]$$

$$\tilde{\mathbf{h}}_2 = [0.2, 0.9, 0.3, 1.0]$$

$$\tilde{\mathbf{h}}_3 = [0.16, 0.545, -0.672, 0.256, 0.095, -0.389]$$

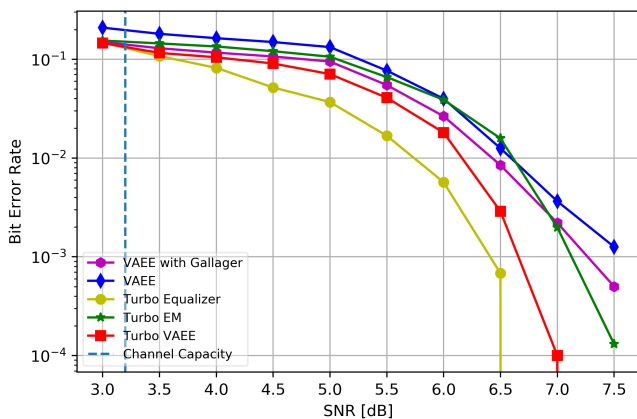
Channel $\tilde{\mathbf{h}}_3$ is taken from [58]. The associated transfer functions are

$$\tilde{H}_1(z) = 0.2 \left(1 + 4.1375z^{-1}\right) \left(1 + 0.3625z^{-1}\right)$$

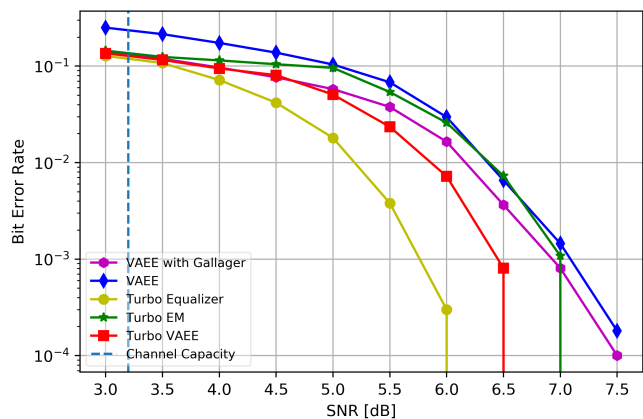
$$\tilde{H}_2(z) = 0.2 \left(1 + 4.4167z^{-1}\right) \left[1 + (0.0417 \pm 1.0632j)z^{-1}\right]$$

$$\tilde{H}_3(z) = 0.16 \left(1 + 4.4241z^{-1}\right) \left(1 - 1.0032z^{-1}\right) \left(1 + 0.6976z^{-1}\right) \left[1 - (0.3561 \pm 0.8115j)z^{-1}\right]$$

The channels $\tilde{\mathbf{h}}_2$ and $\tilde{\mathbf{h}}_3$ have zeros close to the unit circle in the Z -plane. These channels are thus harder to estimate. Figs. 12, 13 and 14 present BER results for the channels $\tilde{\mathbf{h}}_1$, $\tilde{\mathbf{h}}_2$ and $\tilde{\mathbf{h}}_3$, respectively, for the two codes with blocklengths N_1 and N_2 . The blind decoding algorithms that were examined include standalone VAAE, standalone VAAE with a Gallager loss term as described in Section V-A, turbo VAAE with a Gallager loss term \mathcal{L}_G component and BP iterations as described in Sections V-A and V-B, and turbo EM. As a practical upper bound on the achievable performance we also plot the BER of the channel informed non-blind turbo equalizer. As can be seen, the new blind turbo VAAE algorithm significantly



(a) LDPC code with blocklength N_1



(b) LDPC code with blocklength N_2

Fig. 12: BER vs. SNR for the blind decoding algorithms and for the channel informed turbo equalizer. The channel is $\tilde{\mathbf{h}}_1$.

outperforms all the other blind decoding algorithms including the baseline turbo EM, and is quite close to the performance of the (non-blind) channel informed turbo equalizer. For the difficult channels, $\tilde{\mathbf{h}}_2$ and $\tilde{\mathbf{h}}_3$ (with zeros close to the unit circle in the Z plane), both standalone VAAE and turbo EM perform poorly. VAAE with Gallager loss performs much better, and an additional significant gain is obtained by using the turbo VAAE algorithm. Finally note that there is a trade-off between VAAE with a Gallager loss and turbo VAAE: While the later performs better, the former requires less computations.

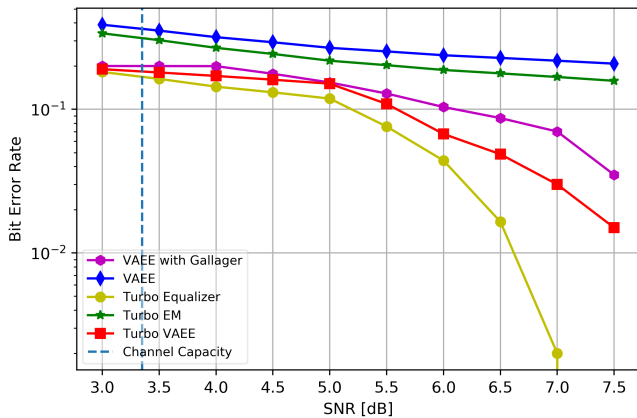
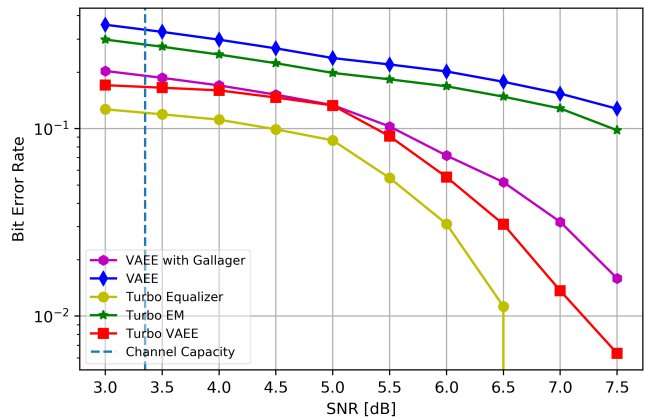
(a) LDPC code with blocklength N_1 (b) LDPC code with blocklength N_2

Fig. 13: BER vs. SNR for the blind decoding algorithms and for the channel informed turbo equalizer. The channel is $\tilde{\mathbf{h}}_2$.

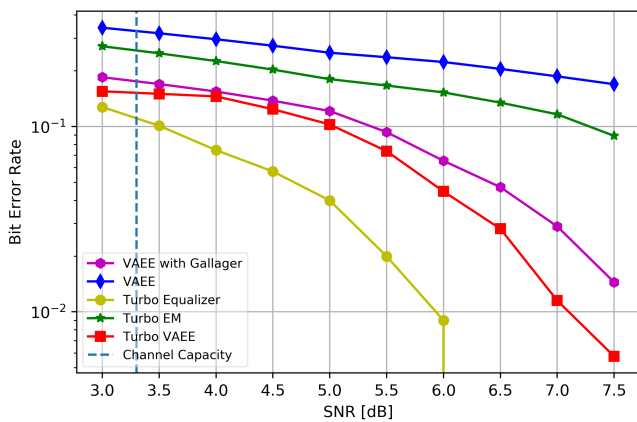
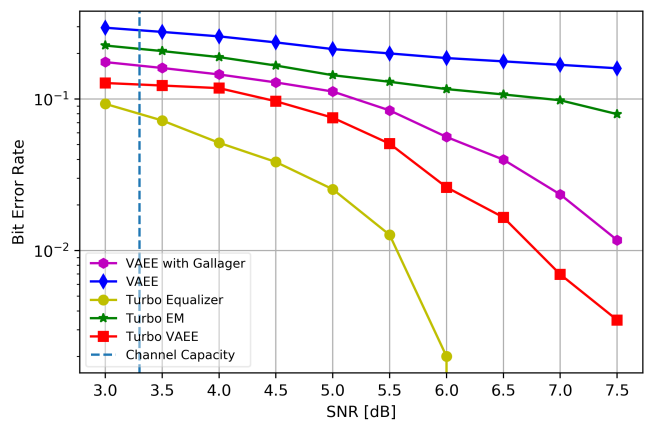
(a) LDPC code with blocklength N_1 (b) LDPC code with blocklength N_2

Fig. 14: BER vs. SNR for the blind decoding algorithms and for the channel informed turbo equalizer. The channel is $\tilde{\mathbf{h}}_3$.

C. Nonlinear channels

We simulated the nonlinear channels as proposed in [25]–[29],

$$g_1(a_n) = \tanh(a_n)$$

$$g_2(a_n) = a_n + 0.2a_n^2 - 0.1a_n^3$$

$$g_3(a_n) = a_n + 0.2a_n^2 - 0.1a_n^3 + 0.5 \cos(\pi a_n)$$

where we define $a_n \triangleq \sum_k x_k h_{n-k}$. It should be noted that $g_2(\cdot)$ and $g_3(\cdot)$ represent an amplifier working in saturation.

As a practical upper bound on the performance, we compared our results to a non-blind turbo equalization algorithm which knows the true channel impulse response \mathbf{h} , the noise variance σ_w^2 and the nonlinearity $g(\cdot)$. This algorithm uses a modified BCJR algorithm which is very similar to the standard BCJR algorithm [24], except that after we have computed the convolution a_n we apply the nonlinear function $g(\cdot)$. That is, we compute $g(a_n)$ and proceed as before. We also compared our turbo VAEE algorithm to the turbo EM algorithm that was used in the previous subsection. This algorithm ignores the nonlinearity. To the best of our knowledge there does not exist any other baseline blind estimation algorithm for the nonlinear case that we could compare with.

In the following simulations, we used the channel $\tilde{\mathbf{h}}_3$, and the same two LDPC codes with blocklengths $N_1 = 576$ and $N_2 = 2304$ that were used in the previous section. The dropout probabilities in Fig. 6, describing the neural network A , were 0.3. The results are presented in Figs. 15, 16 and 17. As can be seen, the new iterative turbo VAEE algorithm significantly outperforms the blind turbo EM algorithm, and is not very far from the performance of the non-blind nonlinear turbo equalizer which is channel informed.

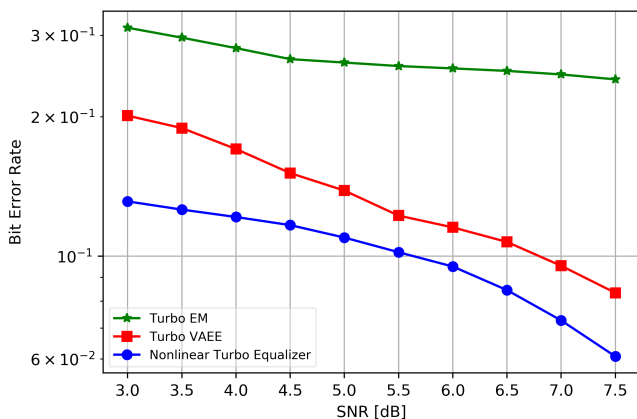
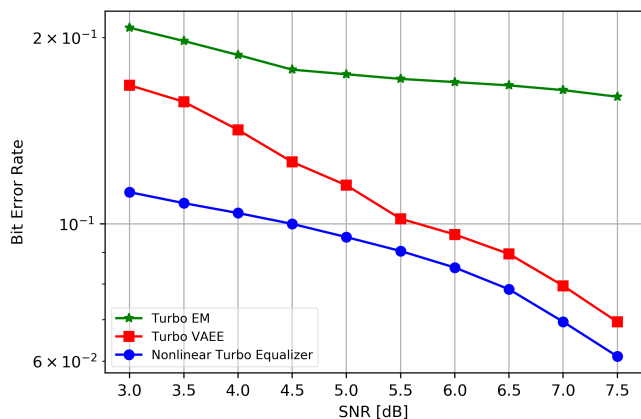
(a) LDPC code with blocklength N_1 (b) LDPC code with blocklength N_2

Fig. 15: BER vs. SNR for the blind decoding algorithms and for the channel informed turbo equalizer. The channel is $\tilde{\mathbf{h}}_3$. The nonlinearity is $g_1(\cdot)$.

VII. CONCLUSION

We introduced novel unsupervised neural network-based algorithms for blind channel equalization using the method of variational autoencoders. Both linear and nonlinear noisy ISI channels were considered. The results were then extended to joint equalization and decoding of LDPC codes using an iterative turbo VAEE algorithm. We showed significantly improved BER performance compared to the baseline algorithms. For LDPC coded data, we demonstrated significantly lower BER values when using turbo

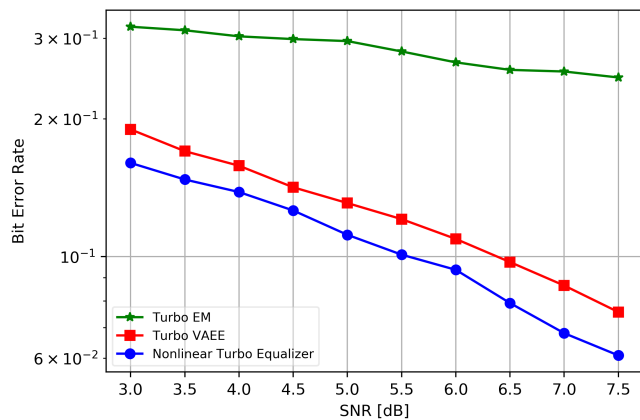
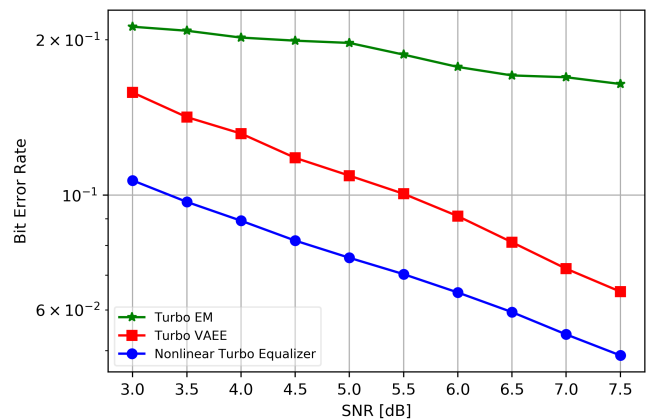
(a) LDPC code with blocklength N_1 (b) LDPC code with blocklength N_2

Fig. 16: BER vs. SNR for the blind decoding algorithms and for the channel informed turbo equalizer. The channel is $\tilde{\mathbf{h}}_3$. The nonlinearity is $g_2(\cdot)$.

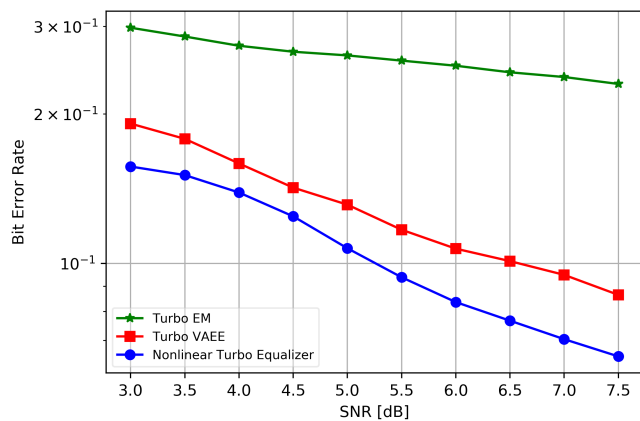
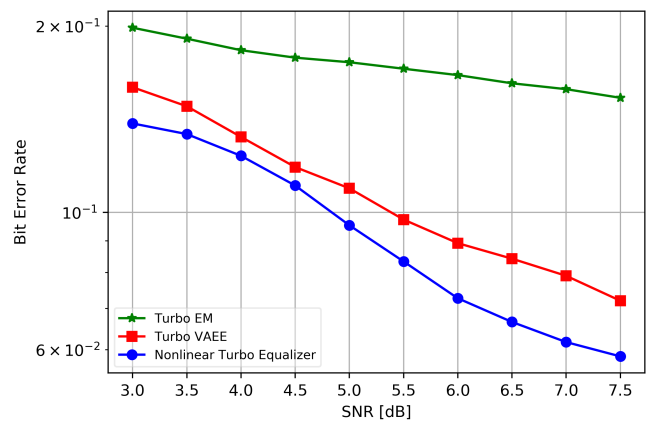
(a) LDPC code with blocklength N_1 (b) LDPC code with blocklength N_2

Fig. 17: BER vs. SNR for the blind decoding algorithms and for the channel informed turbo equalizer. The channel is $\tilde{\mathbf{h}}_3$. The nonlinearity is $g_3(\cdot)$.

VAAE compared to the baseline turbo EM algorithm. In fact, the performance of the new iterative turbo VAAE decoder was not far from the performance of the non-blind channel informed turbo equalizer which is based on the BCJR algorithm. Furthermore, the computational complexity of turbo EM is exponentially increasing in the length of the estimated channel impulse response, since it uses a trellis-based equalizer, where the number of states grows exponentially with the length of the estimated impulse response. Turbo VAAE, on the other hand, uses a simple fully convolutional neural network. Future research should extend our method to generalized setups such as higher constellations and channel acquisition for massive MIMO.

REFERENCES

- [1] E. Nachmani, Y. Be'ery, and D. Burshtein, "Learning to decode linear codes using deep learning," in *54'th Annual Allerton Conf. On Communication, Control and Computing*, September 2016, pp. 341–346.
- [2] E. Nachmani, E. Marciano, L. Lugosch, W. J. Gross, D. Burshtein, and Y. Be'ery, "Deep learning methods for improved decoding of linear codes," *IEEE Journal of Selected Topics in Signal Processing*, vol. 12, no. 1, pp. 119–131, 2018.
- [3] T. Gruber, S. Cammerer, J. Hoydis, and S. ten Brink, "On deep learning-based channel decoding," in *Conference on Information Sciences and Systems*, 2017.
- [4] S. Cammerer, T. Gruber, J. Hoydis, and S. ten Brink, "Scaling deep learning-based decoding of polar codes via partitioning," in *IEEE Global Communications Conference (GLOBECOM)*, 2017, pp. 1–6.
- [5] T. O'Shea and J. Hoydis, "An introduction to deep learning for the physical layer," *IEEE Transactions on Cognitive Communications and Networking*, vol. 3, no. 4, pp. 563–575, 2017.
- [6] N. Samuel, T. Diskin, and A. Wiesel, "Deep MIMO detection," in *IEEE 18th International Workshop on Signal Processing Advances in Wireless Communications (SPAWC)*, Sapporo, Japan, July 2017.
- [7] N. Farsad and A. Goldsmith, "Neural network detection of data sequences in communication systems," *IEEE Transactions on Signal Processing*, vol. 66, no. 21, pp. 5663–5678, November 2018.
- [8] F. Liang, C. Shen, and F. Wu, "An iterative BP-CNN architecture for channel decoding," *IEEE Journal of Selected Topics in Signal Processing*, vol. 12, no. 1, pp. 144–159, 2018.
- [9] H. Ye, G. Y. Li, B.-H. Juang, and K. Sivanesan, "Channel agnostic end-to-end learning based communication systems with conditional GAN," in *IEEE Global Communications Conference (Globecom workshops)*, 2018, pp. 1–5.
- [10] T. J. O'Shea, T. Roy, and N. West, "Approximating the void: Learning stochastic channel models from observation with variational generative adversarial networks," in *2019 International Conference on Computing, Networking and Communications (ICNC)*, 2019, pp. 681–686.
- [11] J. G. Proakis and M. Salehi, *Digital communications*, 5th ed. McGraw-Hill Education, 2007.
- [12] D. Godard, "Self-recovering equalization and carrier tracking in two-dimensional data communication systems," *IEEE Transactions on Communication*, vol. 28, no. 11, pp. 1867–1875, 1980.
- [13] J. Treichler and B. Agee, "A new approach to multipath correction of constant modulus signals," *IEEE Transactions on Acoustics, Speech, and Signal Processing*, vol. 31, no. 2, pp. 459–472, 1983.
- [14] R. Johnson, P. Schniter, T. J. Endres, J. D. Behm, D. R. Brown, and R. A. Casas, "Blind equalization using the constant modulus criterion: A review," *Proceedings of the IEEE*, vol. 86, no. 10, pp. 1927–1950, 1998.
- [15] C. You and D. Hong, "Nonlinear blind equalization schemes using complex-valued multilayer feedforward neural networks," *IEEE Transactions on Neural Networks*, vol. 9, no. 6, pp. 1442–1455, 1998.
- [16] M. Ghosh and C. L. Weber, "Maximum-likelihood blind equalization," *Optical Engineering*, vol. 31, no. 6, pp. 1224–1229, 1992.
- [17] L. Tong and S. Perreau, "Multichannel blind identification: From subspace to maximum likelihood methods," *Proceedings of the IEEE*, vol. 86, no. 10, pp. 1951–1968, 1998.
- [18] H. A. Cirpan and M. K. Tsatsanis, "Maximum likelihood blind channel estimation in the presence of doppler shifts," *IEEE Transactions on Signal Processing*, vol. 47, no. 6, pp. 1559–1569, 1999.
- [19] G. K. Kaleh and R. Vallet, "Joint parameter estimation and symbol detection for linear or nonlinear unknown channels," *IEEE Transactions on Communications*, vol. 42, no. 7, pp. 2406–2413, 1994.
- [20] J. Gunther, D. Keller, and T. Moon, "A generalized BCJR algorithm and its use in iterative blind channel identification," *IEEE Signal Processing Letters*, vol. 14, no. 10, pp. 661–664, 2007.
- [21] X. Wang and R. Chen, "Blind turbo equalization in Gaussian and impulsive noise," *IEEE Transactions on Vehicular Technology*, vol. 50, no. 4, pp. 1092–1105, 2001.
- [22] J. H. Gunther, M. Ankapura, and T. K. Moon, "A generalized LDPC decoder for blind turbo equalization," *IEEE Transactions on Signal Processing*, vol. 53, no. 10, pp. 3847–3856, Oct. 2005.

- [23] A. P. Dempster, N. M. Laird, and D. B. Rubin, "Maximum likelihood from incomplete data via the EM algorithm," *Journal of the Royal Statistical Society: Series B*, vol. 39, no. 1, pp. 1–22, 1977.
- [24] L. Bahl, J. Cocke, F. Jelinek, and J. Raviv, "Optimal decoding of linear codes for minimizing symbol error rate," *IEEE Transactions on information theory*, vol. 20, no. 2, pp. 284–287, 1974.
- [25] B. Mitchinson and R. F. Harrison, "Digital communications channel equalization using the kernel adaline," *IEEE Transactions on Communications*, vol. 50, no. 4, pp. 571–576, 2002.
- [26] J. C. Patra, P. K. Meher, and G. Chakraborty, "Nonlinear channel equalization for wireless communication systems using Legendre neural networks," *Signal Processing*, vol. 89, no. 11, pp. 2251–2262, 2009.
- [27] P. M. Olmos, J. J. Murillo-Fuentes, and F. Pérez-Cruz, "Joint nonlinear channel equalization and soft LDPC decoding with Gaussian processes," *IEEE Transactions on Signal Processing*, vol. 58, no. 3, pp. 1183–1192, 2010.
- [28] H. Ye and G. Y. Li, "Initial results on deep learning for joint channel equalization and decoding," in *2017 IEEE 86th Vehicular Technology Conference (VTC-Fall)*, 2017, pp. 1–5.
- [29] W. Xu, Z. Zhong, Y. Be'ery, X. You, and C. Zhang, "Joint neural network equalizer and decoder," in *15th International Symposium on Wireless Communication Systems (ISWCS)*, Aug. 2018, pp. 1–5.
- [30] A. Caciularu and D. Burshtein, "Blind channel equalization using variational autoencoders," in *2018 IEEE International Conference on Communications Workshops (ICC Workshops)*, Kansas City, MO, May 2018.
- [31] D. P. Kingma and M. Welling, "Auto-encoding variational Bayes," in *International Conference on Learning Representations*, 2014.
- [32] D. J. Rezende, S. Mohamed, and D. Wierstra, "Stochastic backpropagation and approximate inference in deep generative models," in *International Conference on Machine Learning*, 2014.
- [33] Y. Gong, X. Hong, and K. F. Abu-Salim, "Adaptive MMSE equalizer with optimum tap-length and decision delay," in *Sensor Signal Processing for Defence (SSPD 2010)*, 2010.
- [34] C. Douillard, M. Jézéquel, C. Berrou, D. Electronique, A. Picart, P. Didier, and A. Glavieux, "Iterative correction of intersymbol interference: Turbo-equalization," *European transactions on telecommunications*, vol. 6, no. 5, pp. 507–511, 1995.
- [35] R. Koetter, A. C. Singer, and M. Tuchler, "Turbo equalization," *IEEE signal processing magazine*, vol. 21, no. 1, pp. 67–80, 2004.
- [36] O. Shalvi and E. Weinstein, "New criteria for blind deconvolution of nonminimum phase systems (channels)," *IEEE Transactions on information theory*, vol. 36, no. 2, pp. 312–321, 1990.
- [37] C. Trabelsi, O. Bilaniuk, Y. Zhang, D. Serdyuk, S. Subramanian, J. F. Santos, S. Mehri, N. Rostamzadeh, Y. Bengio, and C. J. Pal, "Deep complex networks," in *Proc. 6th Int. Conf. on Learning Representations (ICLR)*, 2018.
- [38] T. J. O'Shea, L. Pemula, D. Batra, and T. C. Clancy, "Radio transformer networks: Attention models for learning to synchronize in wireless systems," in *50th Asilomar Conference on Signals, Systems and Computers*, 2016, pp. 662–666.
- [39] K. He, X. Zhang, S. Ren, and J. Sun, "Deep residual learning for image recognition," in *IEEE Conference on Computer Vision and Pattern Recognition*, 2016, pp. 770–778.
- [40] N. Srivastava, G. Hinton, A. Krizhevsky, I. Sutskever, and R. Salakhutdinov, "Dropout: a simple way to prevent neural networks from overfitting," *The Journal of Machine Learning Research*, vol. 15, no. 1, pp. 1929–1958, 2014.
- [41] A. Mnih and K. Gregor, "Neural variational inference and learning in belief networks," in *International Conference on Machine Learning (ICLR)*, 2014.
- [42] A. Mnih and D. J. Rezende, "Variational inference for Monte Carlo objectives," in *International Conference on Machine Learning (ICLR)*, 2016.
- [43] C. J. Maddison, A. Mnih, and Y. W. Teh, "The concrete distribution: A continuous relaxation of discrete random variables," in *International Conference on Learning Representations*, 2017.
- [44] E. Jang, S. Gu, and B. Poole, "Categorical reparameterization with Gumbel-Softmax," in *International Conference on Learning Representations*, 2017.
- [45] E. J. Gumbel, "Statistical theory of extreme values and some practical applications," *Nat. Bur. Standards Appl. Math. Ser.* 33, 1954.
- [46] R. D. Luce, *Individual Choice Behavior*. John Wiley, 1959.

- [47] R. G. Gallager, "Low density parity check codes," *IEEE Transactions on Information Theory*, vol. 8, pp. 21–28, January 1962.
- [48] T. Richardson and R. Urbanke, *Modern Coding Theory*. Cambridge, UK: Cambridge University Press, 2008.
- [49] L. Lugosch and W. J. Gross, "Learning from the syndrome," in *2018 52nd Asilomar Conference on Signals, Systems, and Computers*, 2018, pp. 594–598.
- [50] M. Abadi, P. Barham, J. Chen, Z. Chen, A. Davis, J. Dean, M. Devin, S. Ghemawat, G. Irving, M. Isard *et al.*, "TensorFlow: A System for Large-Scale Machine Learning," in *12th {USENIX} Symposium on Operating Systems Design and Implementation ({OSDI} 16)*, 2016, pp. 265–283.
- [51] M. Helmling, S. Scholl, F. Gensheimer, T. Dietz, K. Kraft, S. Ruzika, and N. Wehn, "Database of Channel Codes and ML Simulation Results," www.uni-kl.de/channel-codes, 2017.
- [52] S. Abrar and A. K. Nandi, "An adaptive constant modulus blind equalization algorithm and its stochastic stability analysis," *IEEE Signal Processing Letters*, vol. 17, no. 1, pp. 55–58, 2010.
- [53] D. Kingma and J. Ba, "Adam: A method for stochastic optimization," in *International Conference on Learning Representations*, 2015.
- [54] S. S. Ranhotra, A. Kumar, M. Magarini, and A. Mishra, "Performance comparison of blind and non-blind channel equalizers using artificial neural networks," in *2017 9'th International Conference on Ubiquitous and Future Networks (ICUFN)*, 2017, pp. 243–248.
- [55] Y. Fang and T. W. S. Chow, "Blind equalization of a noisy channel by linear neural network," *IEEE transactions on neural networks*, vol. 10, no. 4, pp. 918–924, 1999.
- [56] S. J. Reddi, S. Kale, and S. Kumar, "On the convergence of Adam and beyond," in *International Conference on Learning Representations*, 2018.
- [57] T. M. Cover and J. A. Thomas, *Elements of Information Theory*, 2nd ed. New York: Wiley, 2006.
- [58] L. Salamanca, J. J. Murillo-Fuentes, and F. Pérez-Cruz, "Channel decoding with a Bayesian equalizer," in *IEEE International Symposium on Information Theory*, 2010, pp. 1998–2002.